Transport in Granular Systems

by

Dawn Marie Wendell

Submitted to the Department of Mechanical Engineering
in partial fulfillment of the requirements for the degree of

Doctor of Philosophy in Mechanical Engineering

at the

MASSACHUSETTS INSTITUTE OF TECHNOLOGY

September 2011

Author .....
Department of Mechanical Engineering
August 26, 2011

Certified by .....
Anette (Peko) Hosoi
Associate Professor
Thesis Supervisor

Accepted by .....
David Hardt
Chairman, Department Committee on Graduate Theses

Transport in Granular Systems

by

Dawn Marie Wendell

Submitted to the Department of Mechanical Engineering
on August 26, 2011, in partial fulfillment of the
requirements for the degree of
Doctor of Philosophy in Mechanical Engineering

Abstract

There are many situations in which a continuum view of granular systems does not fully capture the relevant mechanics. In order for engineers to be able to design systems for transporting granular materials, there needs to be an understanding of the mechanics of granular systems and how their non-continuous behavior affects their dynamics. This thesis takes an example of a granular system from nature and uses this system to analyze the way granular materials interact with flexible boundaries.

This thesis focuses on digging in granular materials. Pinto bean plant roots were used as a model biological system, and experiments using photoelastic grains were performed to quantify the effect of the inhomogeneous forces in the substrate on the root growth. It was determined that the pinto bean roots grew between grains when the force between those grains was less than 0.5 N. This value was time-dependent and showed a previously-unquantified strengthening of the roots over time. Also, while the roots were growing in the granular substrate, they altered the forces between grains by an average of 110 mN.

An analytical model of digging energy was developed to investigate the differences between diggers that are much larger than the grain size and diggers that are much smaller than the grain size. Based on this model, a design tool was created so that designers could quickly identify promising technologies for digging based on the size scale of the grains and the desired size of the digger.

Finally, two elements of the plant roots, mechanical flexibility and an actuated tip, were used to create robotic diggers to quantify the associated savings in digging energy. Increasing the mechanical flexibility of the digger was shown to result in energy savings of more than 50% when decreasing the bending modulus by one order of magnitude. However, large variations in the data were observed as a result of the inhomogeneity of the granular system. These variations were quantified and were consistent with previous literature regarding forces in granular systems. Also, a numerical model was created that demonstrates that the increase in digging efficiency

can be attributed to the flexibility of the digger. Experiments with diggers whose tip orientation cycled from side to side show that it is more energy-efficient to dig with this active tip only if the energy used to create the changing tip orientation is less than 2.5×10^{-5} J per mm dug.

Thesis Supervisor: Anette (Peko) Hosoi
Title: Associate Professor

Acknowledgments

This thesis would not have been possible without the help of many people.

First of all, the teacher in middle school who got me started on my way: Mrs. Millar. Next, those in high school who sparked my passion for science and engineering: Mr. Myers, Dr. Waldinger, Dr. Fowler, and the Otis engineers: Jim Rivera, Jim Flood, Ronnie Thibault, Nigel Morris, and Dan Tripp. Once I made it to MIT, I found a whole other group of people ready to push me. My professors showed me what drive truly is: Prof. Boyce, Prof. McKinley, Prof. Culpepper, Prof. Blanco, and many others.

But I owe my graduate career to a very few people who believed in me before I believed in myself. First of all, Prof. Hunter, who was the first person to ever tell me that I should get a PhD. Prof. Abeyaratne, whose quiet leadership convinced me to stay when I wanted to leave. And Prof. Hosoi, who took me on as a PhD student after I spent an entire semester of 2.006 in her office many years earlier. Prof. Hosoi's can-do attitude and insightful critiques of my work have inspired me to be a better researcher every day. I will greatly miss our weekly research meetings.

I especially have to thank my wonderful committee members for challenging me to do great work: Prof. Pedro Reis, Prof. Carol Livermore, and Dr. Julio Guerrero. I've also had several great UROPS to help me with my work, especially Katharine Luginbuhl.

I was lucky enough to have fantastic friends to see me through: Amy, Barbara, Tanya, Bryan, Sungyon, Tony, Brian, Daniel, Randy, Amos, Justin, Nadia, Lisa, Sarah, Ahmed, Thomas, Nic, Rachel, and Jennifer. And of course, my family, who has always supported my crazy engineering dreams.

And Diego - thank you for loving and supporting me no matter what.

Contents

List of Figures

List of Tables

Chapter 1

Introduction

Introductory engineering classes tend to lump materials into several specific categories. Fluid mechanics and solid mechanics are taught as separate, distinguishable subjects and systems are made to fit into one mold or the other. However, the class of granular systems is hard to categorize using such rigid metrics. In some situations, like avalanches, grains flow like a liquid [37]. The shape and collapse of sand dunes is governed by the properties of the sand grains they are built from [2, 37]. But looking at a sand castle on the beach, those same grains appear to be much more solid that the sand avalanche from a collapsing dune. Granular systems can exhibit complex combinations of properties of both solids and liquids [11, 39].

In addition to the granular systems found in nature, there are many engineering systems with granular elements. Grain silos are a common example of a system that has to be designed for the peculiar behaviors inherent in granular systems. Sometimes in silos, the grains from the top of the silo are unable to flow to the bottom of the silo because of an effect called bridging [79]. When this occurs, the weight of the grains at the top of the silo are transmitted to the walls of the silo with a larger component of force normal to the silo walls than typically expected from weight of grains. This can cause large-scale failure of the grain silos [18], as shown in Figure 1-1a [6].

Another common granular system arises in the pharmaceutical industry. Production of medication in pill form is a multi-billion dollar industry. However, the automated handling of these medications involves complex manufacturing systems.

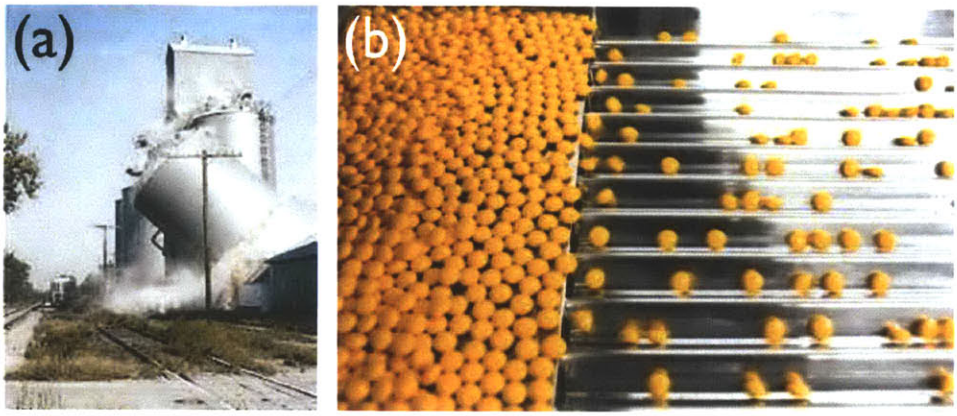

Figure 1-1: (a) Grain silo collapse from [6] and (b) a sorting step in the manufacture of pharmaceuticals from [58].

Efficiency and accuracy of the automated systems requires an understanding of transport of granular systems. However, most of the production and patents for handling such granular systems are based on trial and error innovation, not a fundamental understanding of the physics of granular transport. Current technologies involve channels and vibrating beds, an example of which is seen in Figure 1-1b.

1.1 Analysis of Granular Systems

In each granular system, there are a variety of different parameters to analyze depending on the specific focus or goal of the research. Some examples include the volume fraction of the grains, the background fluid around the grains (air, water, oil, etc.), and the speed at which the grains are moving (either relative to one another or relative to a surface). Each of these different parameters can drastically change the system dynamics. To investigate granular systems, research is often performed using a variety of analytical and experimental techniques.

1.1.1 Experimental Techniques for Granular Research

The non-Newtonian behaviors of granular suspensions was studied most famously by Bagnold [3, 4]. Starting from Bagnold's observations of sand dunes, many others

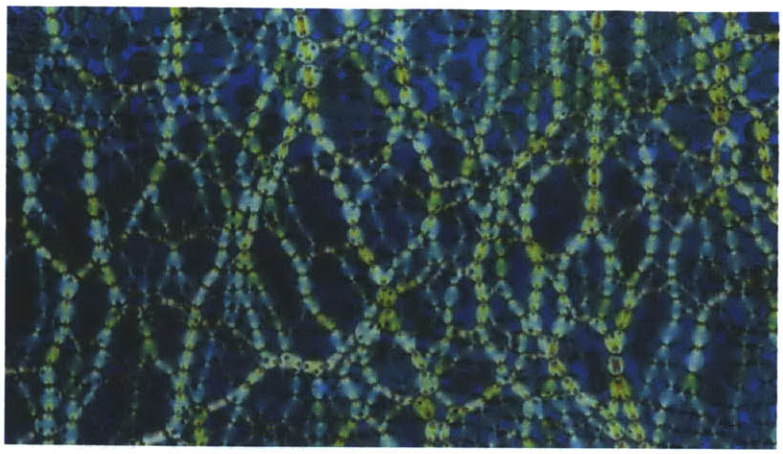

Figure 1-2: Force chains in a photoelastic granular material, from [74].

have studied granular systems in geometries such as granular piles [28], simple shear [35, 47, 54, 56], cyclic shear [75], and slow drag [27]. The experimental techniques are often common to other areas of engineering and physics. Photographic tracking of individual particles can be performed, similar to Particle Image Velocimetry (PIV) in fluid systems. Also, forces can be experimentally observed using photoelasticity, a stress visualization technique from solid mechanics. By observing the birefringence of individual grains, the stress on the grain is quantified. This method has been used extensively in the lab of Prof. Robert Behringer at Duke University [6] to investigate the force on individual grains in a variety of experimental geometries.

1.1.2 Analytical Techniques for Granular Research

The saturation level of the system and volume fraction of the grains leads to different analytical modeling techniques, from fluid dynamics equations to computational simulations. First, at low volume fractions, well below the random loose packing limit, and suspended in a background fluid such as water or oil, many granular systems can be well-described using a non-Newtonian or modified viscosity equivalent viscosity [67, 29]. The system dynamics are computed with fluid dynamics equations simply by using the equivalent viscosity and neglecting the inter-particle interactions. However, at packing fractions approaching the random loose packing limit, the grains

begin to interact with other grains, not just surrounding fluid, and the equivalent non-Newtonian viscosity ceases to model the system interactions well.

In systems with large numbers of interacting grains, modeling of each individual grain and its interactions with neighbors can well-describe the system dynamics. This can be done analytically by taking into account the forces and dynamics of individual particles and groups of particles (for example [19, 22]). An entire class of computer programs have been created to help simulate these systems. Called Discrete Element Models (DEM), the software uses simple contact dynamics and force and torque balance to calculate the position and force of each particle. Although computationally-intensive for large numbers of grains and sensitive to the pre-defined boundary conditions of the simulation, these sorts of models are being used for a variety of research simulations with thousands of particles [64].

1.2 Biologically-Inspired Granular Systems

In order to understand how to design mechanical systems to interact with granular substrates, engineers often look to biology to try to discover new, efficient mechanisms from biological creatures that have been optimized through evolution to interact with these environments. Two examples that have been investigated previously are sandfishes and worms.

The sandfish, scincid lizard genus *Scincus*, has been studied for its intriguing behavior of swimming through desert sand. In this dry granular media, it buries itself into the sand and then undulates its body to slide through the sand. Although there are conflicting reports about the use of its appendages during this swimming motion [5, 49], the sandfish is now being used as a model for new robotic sandswimmers using the primary large-amplitude traveling wave oscillations [48] with applications for exploration and reconnaissance.

Small *C.elegans* worms traveling through water-saturated beach sand take advantage of their environment in a similar way. The *C.elegans* are close in size to the diameter of the grains, so each grain is a significant obstacle. However, in swimming

experiments with water and glass beads, the worms travel faster in a substrate that includes grains [40]. This unexpected observation is explained by the more asymmetric drag on a slender body provided by the grains. Clearly the *C.elegans* worms are using their usual habitat to their advantage in their swimming strategy.

Investigating biology can lead to discoveries about how to optimize interactions with granular materials and also elucidate physical properties of the grains that might otherwise be overlooked. It is important to continue to use biology for inspiration when analyzing the dynamics of granular system.

1.3 Biologically-Inspired Transport in Granular Systems

This thesis focuses on transport in granular systems. The primary morphology investigated is digging. The biological inspiration for the digging research comes from plant root growth. Plant roots are mechanically flexible intruders into granular beds. Plant root growth has been studied in the agriculture [1, 8, 9, 20] and biology communities [15, 21, 55] but no work has been done to address grain-scale force inhomogeneities in granular systems and study their effects on plant roots. This thesis investigates plant root growth through a system of photoelastic grains and then tests the digging energetics of two associated mechanical motions derived from the plant root growth. Using a photoelastic substrate allows for quantitative force measurements at all points in the system during root growth. After quantifying the ability of plant roots to grow through granular substrates, two elements of the plant roots were used to create robotic diggers: mechanical flexibility and tip reorientation. These robotic diggers were characterized by the energy required for digging in a dry glass bead substrate. A numerical model was developed to gain insight into the essential physical mechanisms that contribute to the energy savings. Also, two models of the energy required for digging in a granular substrate were proposed, one for a continuum model of granular systems and one for a discrete model. A Matlab tool for selecting MEMS actuators

for use in digging robots was created using these digging energy models.

Also, a preliminary investigation into experimental modeling the small intestine as a granular slurry system is reported in Appendix A. The primary motion from the small intestine, peristalsis [72, 34], is modeled experimentally via peristaltic pumping. Previous work in peristaltic pumping has focused on the pumping characteristics of Newtonian fluids [63, 38, 13, 60, 69, 73] and created numerical models for peristaltic pumping of non-Newtonian fluids [12, 43, 44, 61, 66] and granular suspensions where the volume fraction of grains is well below the random loose packing limit [36, 53, 67]. However, none of this work addresses situations where the volume fraction of grains is high enough for the grains to interact with each other during peristalsis. This dense-grain regime is investigated as another example of a system where the granularity of the substrate affects the dynamics.

Chapter 2

Biological Inspiration for Digging In Granular Materials

When digging through granular materials, there are several different regimes that can be considered based on the ratio of the digger size to substrate grain size, and the amount that the digger changes its shape in response to the environment (which will be referred to as the responsiveness to the environment). For example, a shovel or auger would be in the regime where the digger is much larger than the grains, and the digger does not change based on their environment. At the opposite extreme, a plant root growing through a rocky soil would be in a situation where the digger (the root) is very responsive to the environment in that it is able to grow around the grains, and the roots are smaller than the rock fragments. Putting a straw into a glass of ice water would be the regime where the digger is not responsive to the environment (assuming that the straw does not buckle while it is pushed through the ice), but the grains are larger than the digger. Finally, a plant growing in a fine soil would be an example of a system where the roots are very responsive to the environment and the grains are smaller than the digger. These regimes are summarized in Figure 2-1.

This research focuses on systems in which the diggers are smaller than the grains with a variety of responsivenesses. Many systems already exist where the diggers are larger than the grains, but with an increase of knowledge about miniaturized robots and an expanding array of MEMS actuators, creating diggers that are smaller than

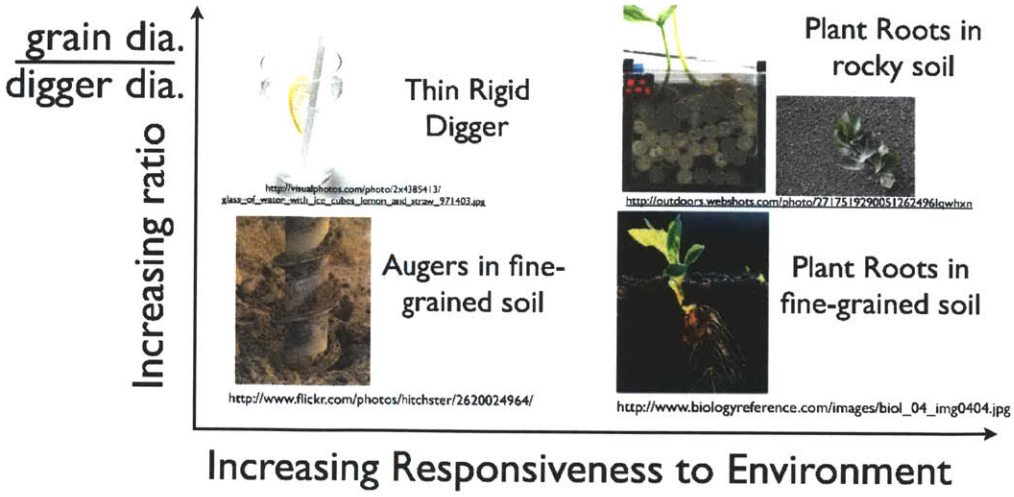

Figure 2-1: Digging regimes based on the size scale of the digger relative to the grain size and the responsiveness of the digger shape to the granular environment.

the grain size is becoming technologically achievable. However, the design parameters used to design such diggers are still unknown. This section will focus on a biological inspiration for digging and the subsequent chapters will include an evaluation of two mechanical digging motions adapted from the biological inspiration system, and the introduction of a new tool for MEMS actuator selection for small-scale digging systems.

2.1 Biological Inspiration

Biology has been finding ways to dig through granular materials for thousands of years. In order to take advantage of the optimization achieved by evolution, a survey of biological systems that dig in granular materials was performed. The results of the survey are summarized in Appendix B. These biological systems have a variety of methods for digging. The biological systems were classified by their size relative to the grain size of the substrates they inhabit, a general description of the digging mechanics used (rigid kinematics, soft materials, etc), and the water content of the soil that they traverse.

The goal of the survey was to find design rules for robotic digging systems that are

smaller than the grain size. Therefore, the biological systems were narrowed down to systems that were small compared to the substrate size. This left two major digging morphologies: worm-like systems and millipede-like systems. Worm-like systems have a long, slender, flexible body. Previous work has showed that the undulation of the worm's body can increase the velocity of the worm when it interacts with grains [40]. Perhaps a similar mechanism could be at play in digging. The millipede-like systems use their small size to an advantage and have many small appendages or legs that allowed them to crawl through the interstitial spaces between grains, much like a rockclimber. Keeping in mind the goal of the project was to develop design rules for robots, simple is better. Therefore, plant roots were selected as the biological system of choice. Plant roots have a worm-like morphology, but they do not have a nervous system so their control algorithms are very simple. Also, they are slow-growing, making observations easier, and they dig in a variety of substrates.

2.1.1 Plant Root Background

This section is adapted from Experimental Investigation of Plant Root Growth Through Granular Substrates *by DM Wendell, K Luginbuhl, J Guererro, and AE Hosoi, submitted to Experimental Mechanics, March 2011.*

Plants grow across the planet, from inhospitable environments in the Sahara desert to tropical rainforests in Central America. Research has shown that roots grow via cellular division in the root tip region [24, 23], however, the mechanics of root growth at the system level are still not well understood. The importance of drainage and aeration are studied for crops [77, 8], but the work in these areas is incomplete because of the lack of knowledge about plant root growth in granular substrates.

Plant root growth has been previously studied extensively in the biological and agricultural communities. However, these literatures neglect the grain-scale inhomogeneities in granular substrates that the physics community has identified and described extensively [16, 28, 45, 47, 54]. Experimental studies of root growth often use agar [21], which is a homogeneous gelatin material, air [65], or soil characterized

by bulk properties [9, 20, 55, 59, 78]. Also, studies on cellular growth neglect system-level morphology of the roots and associated applications for growth and digging [15].

This section describes the application of a mechanical visualization technique, photoelasticity, applied to the investigation of inter-grain force effects on the growth of pinto bean root systems. Photoelasticity is the observation of two distinct indices of refraction resulting from applied mechanical stress. These dual indices of refraction can be visualized using polarized light, where the intensity of the transmitted light provides a quantitative measure of the stresses in the material [52]. Previous studies have used photoelasticity to observe the stresses in two pinned grains as a chickpea root grows through a gap between the grains [41]. These innovative experiments investigated the effect of the distance between grains on root growth, as well as the initial force the root exerted on the fixed grains during its first ten hours of growth. To complement this earlier work, the apparatus described here was designed to investigate longer-term behavior of systems with dozens of grains that are unpinned and in contact with each other, allowing for system-level rearrangements during root growth. Using the apparatus and this photoelastic technique for stress visualization, two topics were analyzed: how plant roots respond to different levels of force between grains in a system, and how the growing roots change the inter-granular forces. The time-variability of these conditions was also investigated.

2.1.2 Experimental Investigation of Plant Root Growth in Granular Materials

An experimental apparatus was designed to simultaneously record the growth of plant roots and instantaneous force data between grains in the granular packing. In order to simplify the experiments, the setup was designed to be two-dimensional. Multiple experiments were run simultaneously. Each experiment included a clear plastic 10cm by 10cm acrylic box, shown in Figure 2-2. The grains were manufactured out of polyurethane rubber (McMaster-Carr [51], part 8787K32) which is biocompatible,

translucent, photoelastic in the visible light spectrum, and sensitive to biologically-relevant force levels (0.1 to 5 N). Grains were machined by waterjet-cutting 3/8" (9.5 mm) disks from the polyurethane sheet 0.25" thick (6.35 mm). Circular polarizing filters were attached to the front and the back of each acrylic box to visualize the inter-grain forces.

A time-lapse camera system was built to record the information from several simultaneous experiments. A camera attached to a Lego Mindstorms kit was programmed to cycle between experiments, taking one picture of each experiment every seventy minutes. The camera was a Canon PowerShot SD700IS [14] which had been modified to run the CHDK camera software [17]. Images were transferred to a computer from the camera every few days to ensure that the memory card did not reach its storage capacity. After the experiments concluded, the images were processed using Matlab [50] as described below.

In order to accurately determine the inter-grain forces, two methods were investigated. The first method was based on the optical birefringence properties of the polyurethane grains, similar to [47]. The intensity of the light passing through the grain is proportional to the force acting on the grain [52]. A calibration was performed using a Micro-Texture Analyzer by Texture Technologies [70]. One grain was subjected to a known force and a photograph was taken so that a correlation between the optical intensity and applied force could be found. However, it was observed that the light intensity vs applied force was not a monotonic function for this material. For this reason, a second method was used to calculate the forces observed in the experiments.

The second method investigated to calculate the inter-grain forces involved counting fringes inside the particles and corresponding that data with the calibration photos taken earlier. Automating the fringe-counting process in Matlab proved difficult so the fringes for each particle were counted manually. The resolution of each measurement was 50 mN.

The method for conducting each experiment was dictated by the biological requirements of the pinto beans. The pinto beans were dried organic beans purchased

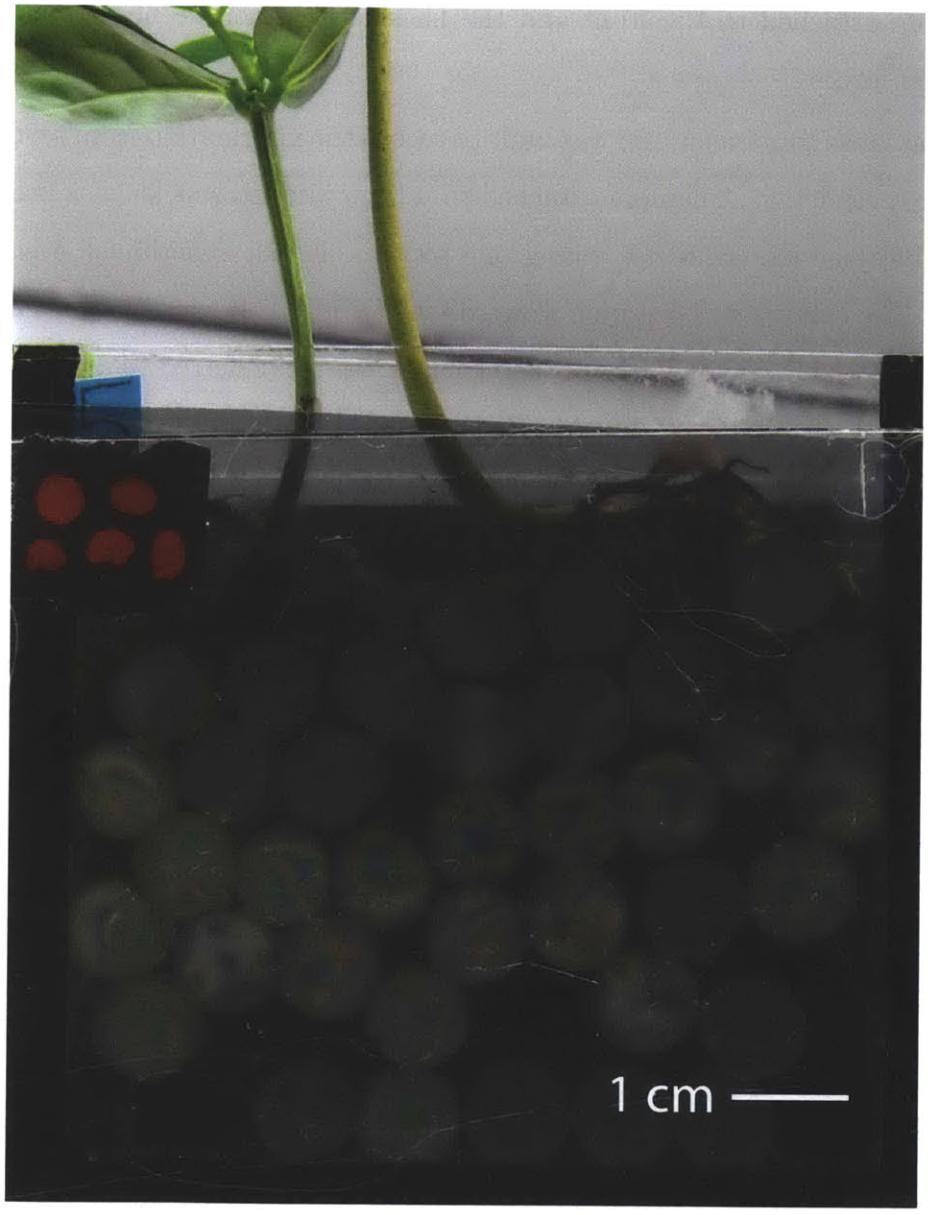

Figure 2-2: Experimental box, filled with polyurethane grains and two pinto bean plants growing inside. The bright fringe patterns in the grains in the center of the image indicate these grains are subject to higher loads than the grains at the top of the box.

from Harvest Cooperative [31] and stored in an open container in a climate-controlled environment. First, approximately twenty pinto beans were sprouted by soaking them in Poland Spring bottled water [71] for 24 hours until they were rehydrated. Poland Spring water was used throughout the experiments because the laboratory tap water is chlorinated. Then the rehydrated beans were placed in a 10-cm diameter petri dish between two pieces of paper towel that were dampened with Poland Spring water. The cover was placed on the petri dish and the dish was left in a dark drawer for 24-48 hours or until the roots began to sprout from the beans.

Next, the acrylic boxes were prepared for the beans. Each box was filled 3/4 full with the polyurethane grains. Care was taken to ensure that the grains remained in a random configuration and did not create a hexagonal packing. Forces were then introduced to the system using a thin piece of plastic to push on the grains until the forces in the system appeared to be well-varied. The box was filled with Poland Spring water until the grains were submerged. Then a sprouted bean was placed in the center of the box, on top of the grains such that the root tip was pointed downwards into the grains. A series of six acrylic boxes were prepared this way, along with a seventh control box. The control box was the same as the other boxes except that it contained no bean and had a thermometer on the front. The control box was used to confirm that the forces in the boxes would not change over time without the presence of a growing bean. The thermometer was used to record the temperature of the experiments. A local temperature reading was necessary because the location of the experiments was near a heat vent and window, so the laboratory thermostat was not an accurate measurement of the experimental conditions.

After setting up the seven acrylic boxes, the computerized camera system was started. Every ten minutes, the motion stage would move to the next experiment box and the camera would take a photograph. Since there were seven boxes, each box was photographed every seventy minutes. To be able to automatically sort which photograph was from which experiment, labels with different numbers of red circles were attached to the front of each experiment so Matlab could automatically sort the images.

The experiments were run for ten to eighteen days with the exact duration depending on plant growth. Experiments ended when the roots stopped growing, the plants died, or the roots had reached the bottom of the acrylic boxes. During the experiments, the plants were watered daily to maintain water in the grains and prevent the roots from drying out. No fertilizer was used in the water. It was apparent that the beans could live for several weeks with only Poland Spring water.

When the experiments ended, the plants were removed from the boxes and the boxes and grains were cleaned with water for the next experiment. No soap was used in order to minimize the number of contaminants with which the plants might come into contact. Then the images were processed using the fringe-counting analysis as described earlier.

Results of Plant Root Growth Experiments

The experimental results of pinto bean growth in granular substrates were used to investigate two questions. First, how do plant roots respond to different levels of force between grains in a system? Secondly, how do the growing roots change the forces between grains in a system?

To determine whether the root's ability to grow between grains was affected by the pre-existing forces between grains, a histogram of root growth versus the inter-grain force was created. Figure 2-3 shows the fraction of roots that grew between grains at a given force, compared to the number of roots that encountered that inter-grain force. The inset in Figure 2-3 shows a histogram of the total number of roots that grew between grains at a given inter-grain force. From this data, it appears that pinto bean roots tend to grow between grains when the force level is less than approximately 0.5 N.

However, we did not observe one cutoff value of inter-grain force which would prevent a root from growing. To determine if the lack of a critical force was due to the inherent variability in the biological system or other factors, the inter-grain forces the growing roots encountered were plotted against time in Figure 2-4. The values of

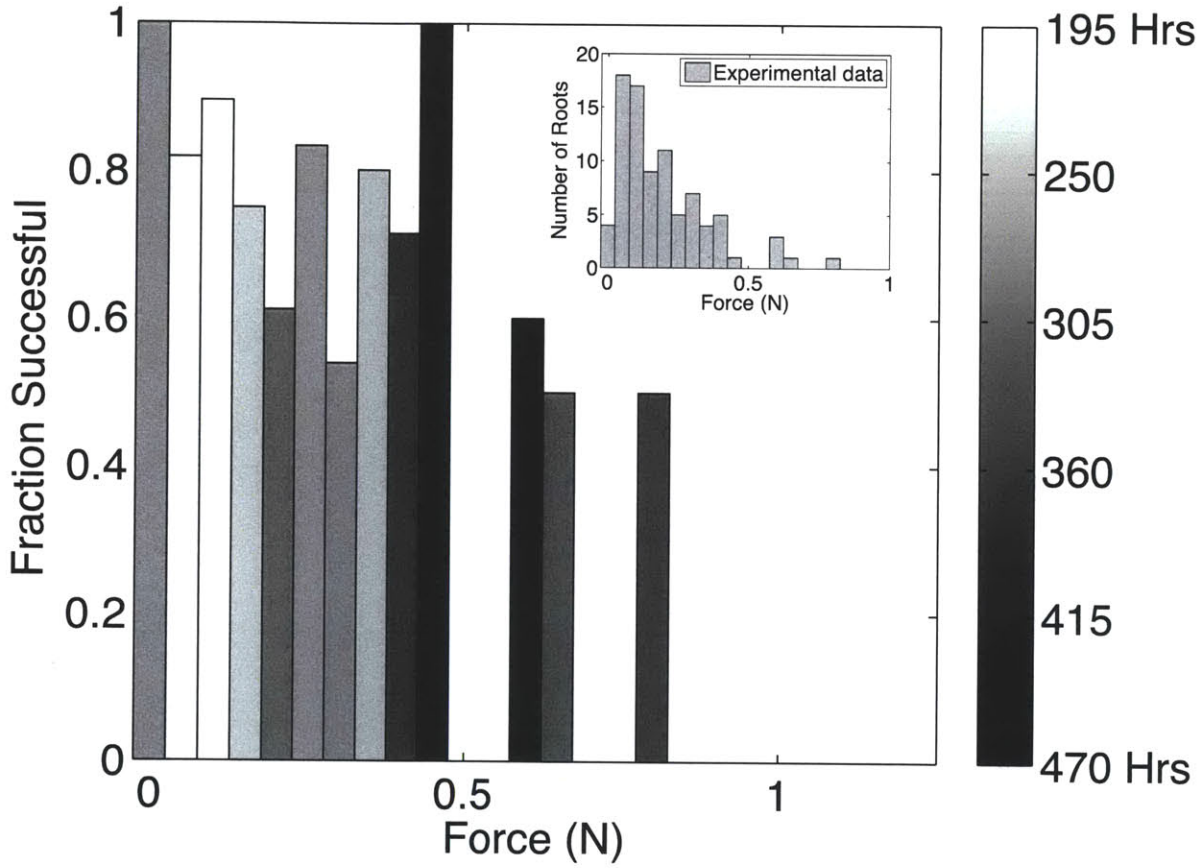

Figure 2-3: The fraction of roots that passed between two grains based on the force between the two grains. The grayscale indicates the average age of roots that were successful, from white (youngest roots) to black (oldest roots). The inset shows the total number of roots that grew between grains for a given inter-grain force.

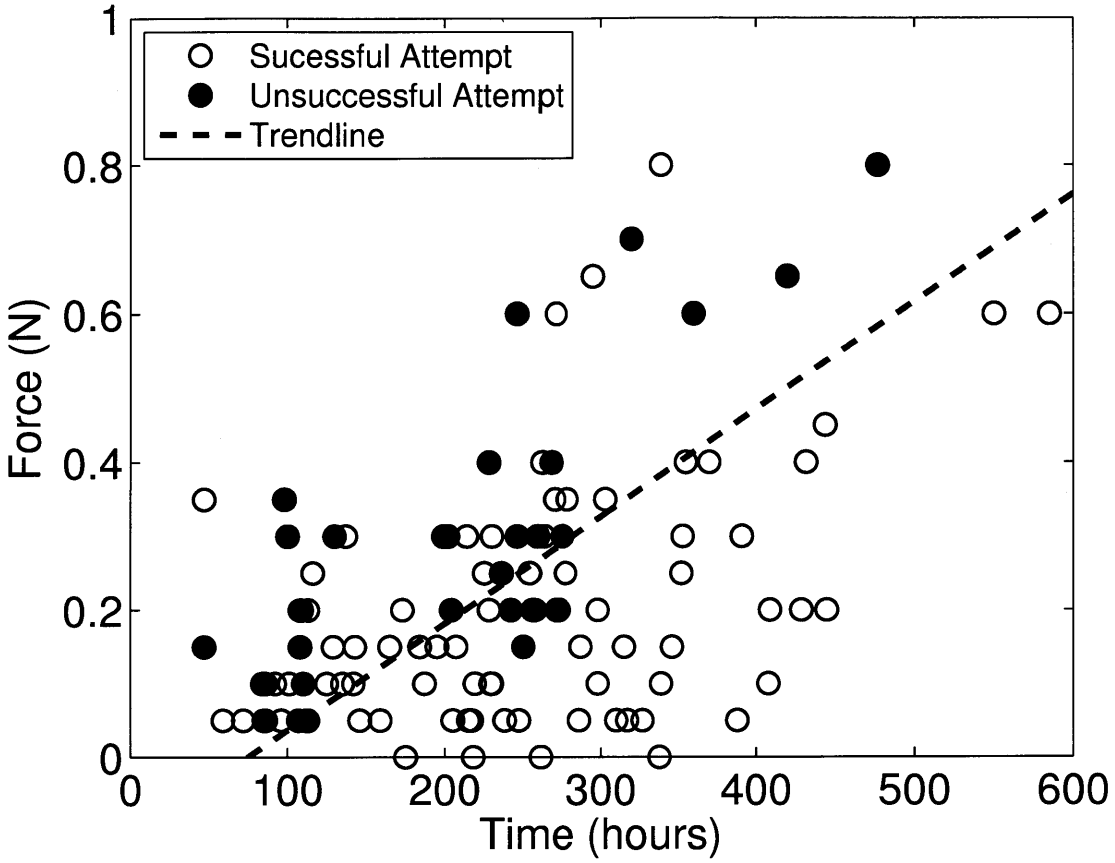

Figure 2-4: The roots ability to grow between grains as a function of the force between the grains and the time of growth. Note that the inter-grain forces that prevented root growth increased over time (ie, the roots became stronger).

inter-grain forces that roots successfully grew through are open circles and values of inter-grain forces that roots did not grow through are filled circles. From this figure, it is clear that the root's growth ability varied as a function of time. Early in time, the roots often did not grow between the grains even when the force between the grains was low. Over time, the limiting inter-grain force increased as shown by the linear trendline, indicating a strengthening of the roots over time. This strengthening is not accompanied by an observable change in root morphology or root branching behavior.

We also observed that the roots affected the stresses within the granular system as they grew between grains (Figure 2-5). This force was interpreted as the force the roots impart to the system and quantified by calculating the change in stress within

Figure 2-5: Roots exerting force into a granular system. Note that the center grain is subject to increasing stresses as the roots grow around it. Time between images is approximately 20 hours.

the grain as the root grew past it. The histogram in Figure 2-6 shows that the pinto bean roots were able to apply an average of 110 mN to the system, with a standard deviation of 65 mN.

The distribution of forces that the roots imparted to the grains was fitted with a Raleigh distribution, which is commonly used to model life expectancy and growth rate in biological systems [62, 25]. Our results are well-described by a Rayleigh probability density function of the form

$$f(x;\sigma) = \frac{x}{\sigma^2} e^{-x^2/2\sigma^2}. \tag{2.1}$$

The x variable describes the range of forces that the roots impart to the grains and σ is a fitting parameter which we find to be 0.0975 N for our experiments. The inset in Figure 2-6 shows the time-dependence of the force that the roots imparted to the grains. The grey diamonds represent the mean of the experimental data and the error bars are the standard error of the mean. The black diamonds represent the experimental data fitted with the Rayleigh distribution and the resulting peak of the distribution is the plotted force level. The vertical error bars are the variance of the modeled probability density function. Once again, a strengthening of the roots over time is observed.

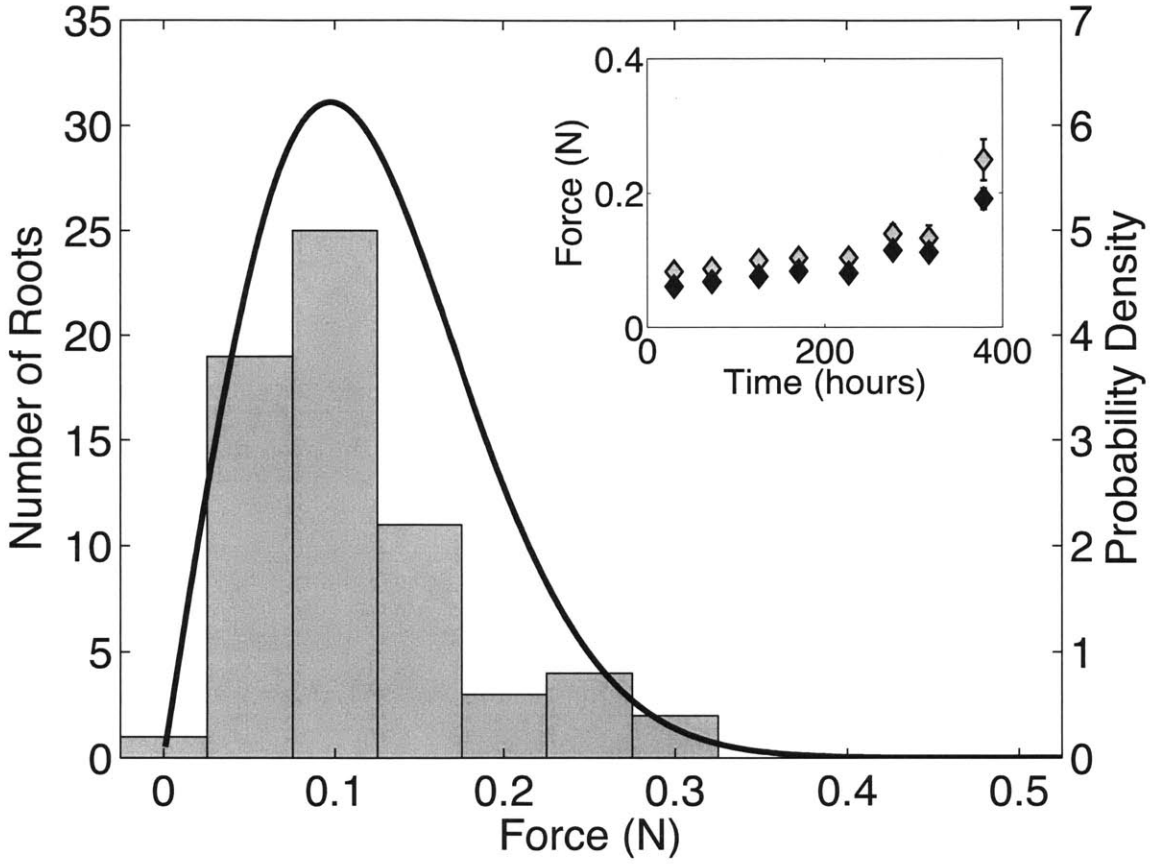

Figure 2-6: A histogram of the forces that the roots applied to the granular system, fitted with a Rayleigh distribution. The inset shows the force that the roots apply to the granular system versus time. The grey diamonds represent the mean of the experimental data. The vertical error bars are standard error of the mean. The black diamonds are the experimental data fitted with a Rayleigh distribution. For each of the points, the histogram of the forces applied by the roots to the system during that time segment of the experiment was fitted with the Rayleigh distribution and the resulting peak of the distribution is the plotted force level. The vertical error bars are the variance of the fitted probability density function. Note that some points do not appear to have error bars because the the error bar is obscured by the size of the point.

In summary, roots are good biological diggers because they are able to avoid obstacles. Although they are limited in the levels of force between grains which they are able to grow through, they are able to take advantage of the different levels of force between grains in a granular system to grow deeper. Two observations that seemed to be most important in the roots' growth was their ability to take tortuous paths (mechanically flexible) and the reorientation of their tip.

Chapter 3

Digging In Granular Materials

The research in the previous chapter on plant root growth in granular materials showed two important elements of plant root growth: the roots' ability to take a non-linear path through the substrate and the changing orientation of the root tip. Both of these elements were investigated separately to increase the understanding of how roots dig in granular materials and to apply the findings to digging robots. The first three sections of this chapter focus on the ability of the root to take a non-linear path due to its flexibility. The investigation into the changing tip orientation is detailed in Section 3.4.

To go deeper than otherwise allowed by their innate strength, the roots take advantage of the inhomogeneities in the granular substrate to find a path of lesser resistance so that they grow past depths where the soil overpressure would be higher than their strength. Mechanical flexibility was used to investigate if it is possible to passively find a path of lesser resistance in a granular substrate, which would lead to energy savings in digging. The goal of these experiment was to use mechanical flexibility to take advantage of stress inhomogeneity in granular materials to develop more efficient digging technologies.

An experimental apparatus was constructed to test the effect of flexibility on the energy required to dig in a granular substrate. The apparatus was designed to be quasi-2-dimensional. The substrate was held by a tall flat box, 150 mm tall and 150 mm wide, 9 mm deep made of clear acrylic plastic. The granular substrate was

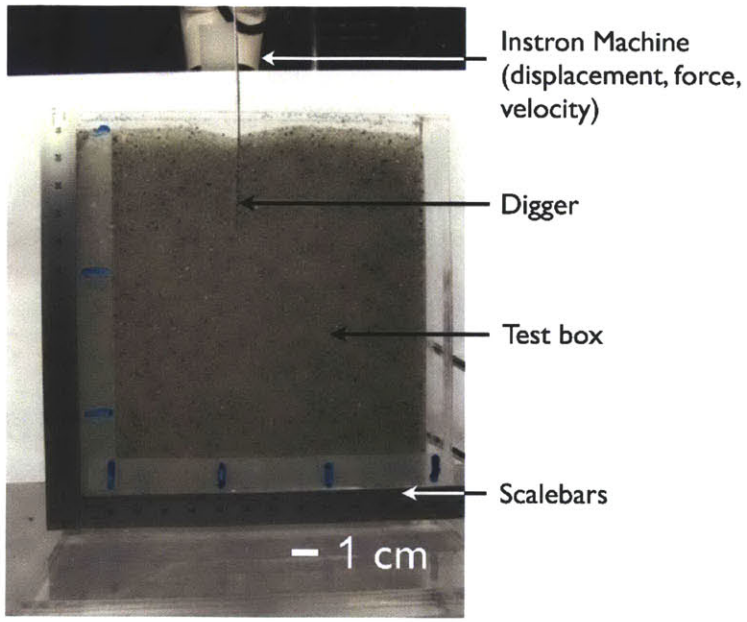

Figure 3-1: Experimental apparatus for flexible digging trials with a granular substrate of soda lime glass beads.

soda lime glass beads, from 1 mm to 2 mm in diameter. The diggers were thin strips of materials, with thicknesses less than the diameter of the smallest grains (the dimensions are summarized in Table 3.1). Similar to the investigated plant roots, the diggers were smaller than the grains so that they could easily move through the spaces between the grains. In the other dimensions, the diggers were about 8 mm wide (so that they could fit into the substrate box without touching the walls which were 9 mm apart), and 125 mm long. The materials used were polycarbonate, aluminum, and steel shim stock, all sold by McMaster-Carr [51].

The experiments were performed with a Micro-Texture Analyzer by Texture Technologies [70]. The digger was clamped in the machine and the substrate box positioned underneath it. The setup is shown in Figure 3-1. The test was run at a constant speed of 1 mm/s. This speed was used for all tests because initial results showed no dependence on speed, as long as the experiments remained in the quasi-static regime. Position and force at the clamp were recorded. The test was performed until the measured force was 0.5 N, at which time the digger was retracted to its starting point. Before each test, the grains were reset so that there would not be any "memory" in

the substrate of previous tests. The grains were dumped out of the substrate box into a plastic cup and then poured slowly back into the substrate box while the box was held on its side at an angle of approximately 20 degrees. The tests were found to be very sensitive to the method of grain preparation, so this method was used for all tests reported here.

The materials used for the diggers and their thicknesses are summarized in Table 3.1. The Young's Modulus of the polycarbonate, aluminum, and steel were 2.2 GPa, 69 GPa, and 200 GPa respectively. Tests were performed with 1 mm grains and 2 mm grains; the substrate grains were monodisperse. Each set of parameters was tested between 5 and 20 times (based on time, material, and machine constraints).

Table 3.1: Flexible Digger Thicknesses in mm

Polycarbonate	Aluminum	Steel
0.254	0.178	0.077
0.318	0.252	0.105
0.381	0.432	0.120
0.508	0.495	0.155
0.635	0.642	0.185
0.762	0.785	0.205
		0.260
		0.312
		0.390

3.1 Results of Experimental Investigation of Flexible Intruders in Granular Packings

After all of the experiments were performed, the results were compared between trials of the same parameters and trials with different parameters. First, plots were made of the results of force versus depth for each parameter set to confirm that the results were consistent. Then all the trials with the same parameters were averaged together and a linear fit line was fitted to the average. A representative sample of such plots are shown in Figure 3-2. The linear fit line represents the average force that is required

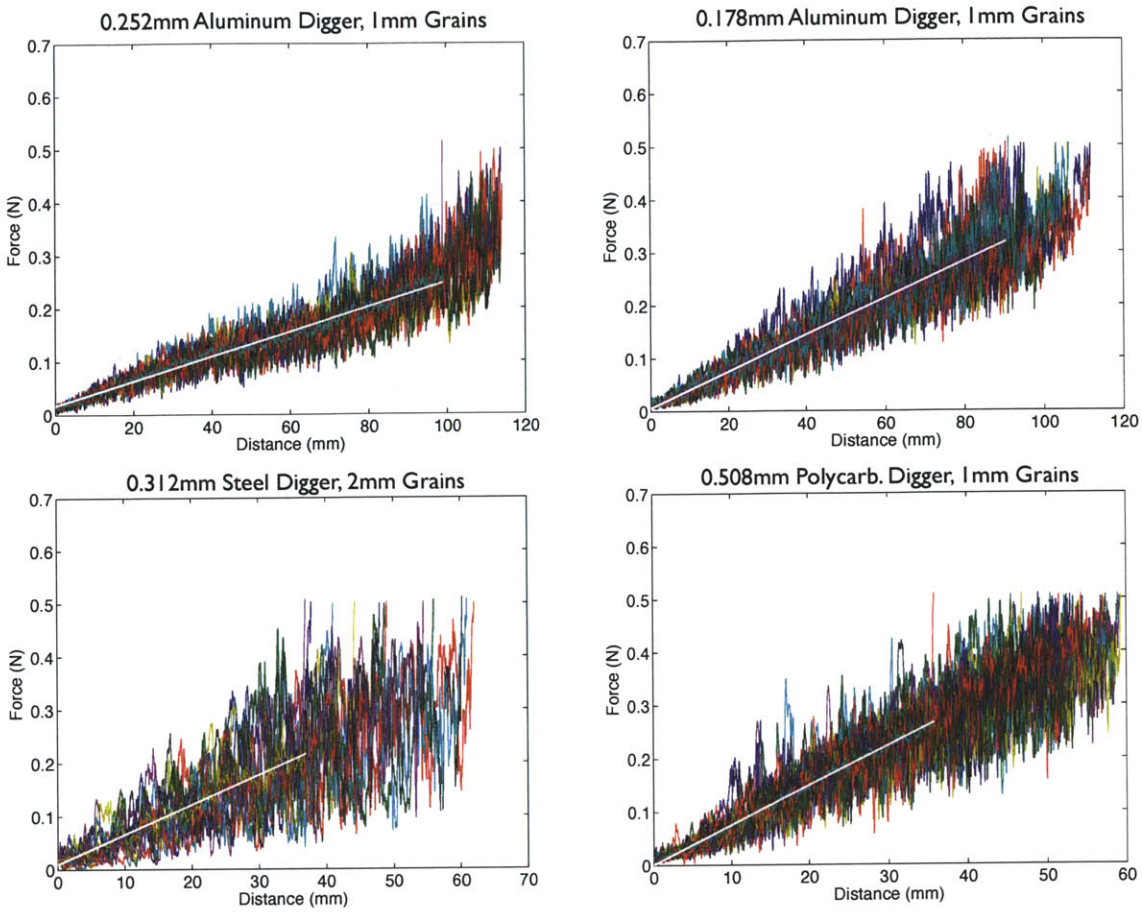

Figure 3-2: Each subplot shows all trials for a given parameter set. The linear fit to the average of all the trials in the graph is plotted in white.

to dig to a certain depth. The energy required to dig to a specific depth can be found by integrating the force required over the digging depth.

To compare different parameters, the linear fit lines for each of the different experiments were plotted together, as shown in Figure 3-3. In this plot, each of the different materials is a different color and the thickness is represented by the darkness or lightness of the colors, where lighter is thinner (ie, more flexible). From this plot, it appears that the lighter lines have a lower slope, meaning less force is required to dig. This same trend can be seen when the digging energy is estimated by integrating the area under the force-depth curves, as shown in Figure 3-4.

Each material can also be evaluated individually to more clearly see the trends relating flexibility to digging energy. The results are shown in Figure 3-5. The

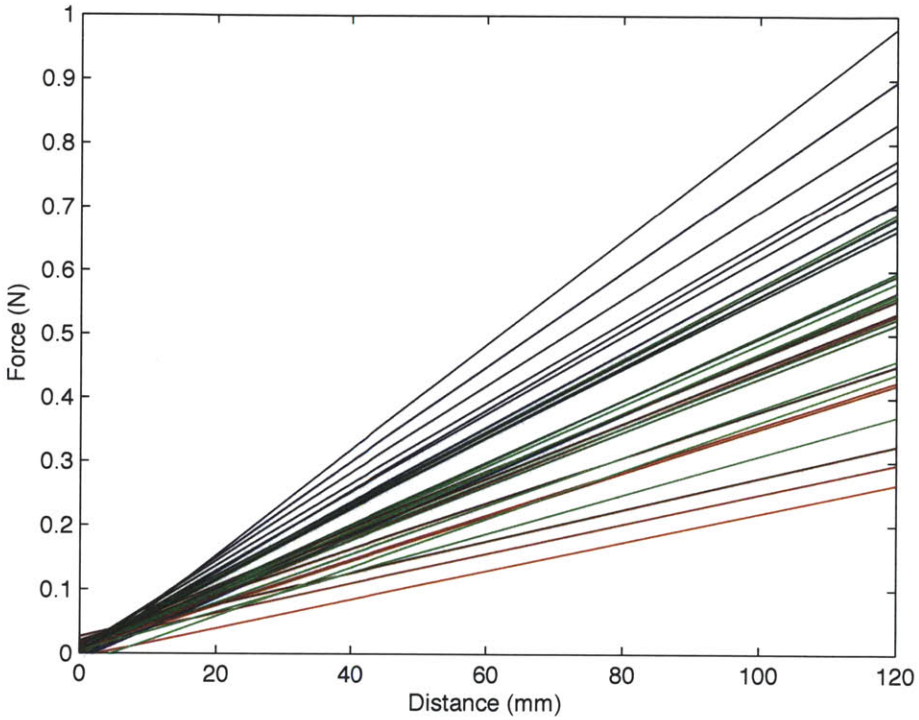

Figure 3-3: Linear fit lines for all parameters. Digger are coded by color: blue is polycarbonate, red is aluminum, green in steel. Thickness of the digger is indicated by the darkness or lightness of the color, where darker this thicker and lighter is thinner. Note that the lighter colored lines tend to have a lower slope, which means less force is required to dig.

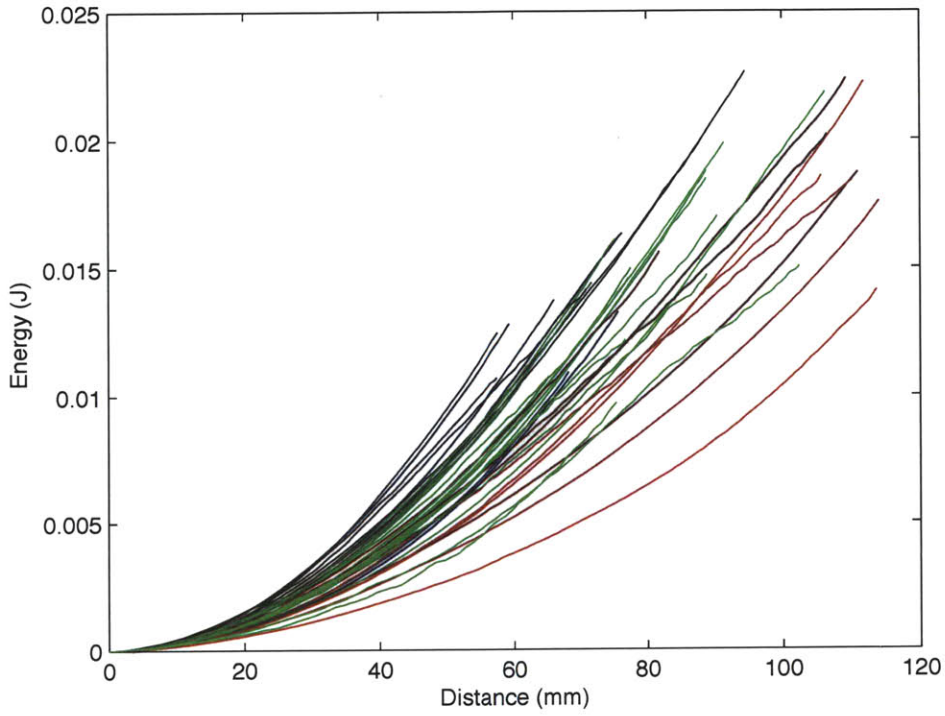

Figure 3-4: Energy required to dig, calculated by integrating the linear fit lines for all parameters. Digger are coded by color: blue is polycarbonate, red is aluminum, green in steel. Thickness of the digger is indicated by the darkness or brightness of the color, where darker this thicker and lighter is thinner. Note that the lighter colored lines tend to be lower on this graph, which means less energy is required to dig.

flexibility of the diggers is indicated by the color bar showing the thickness of the diggers. The thicker the digger, the stiffer the digger because flexibility is quantified by $EI = Eht^3/12$, where E is the Young's Modulus of the digger and I is the bending moment of inertia, $I = ht^3/12$ where t is the thickness and h is the depth in the perpendicular direction.

Another way to evaluate the energy required for digging is to compare the slopes of the linear fit lines from the force versus depth plot (Figure 3-3). The energy for digging is the area under the force versus depth curve. The slopes of the fit lines versus the digger flexibility are plotted in Figure 3-6. All of the materials show the same trend: increasing flexibility decreases the energy required for digging by more than 50%. This decrease in digging energy based on increased flexibility is significant because flexibility is a passive mechanism and can lead to considerable energy savings.

The information gained from the experiments regarding digging force can be used for design of digging systems. For example, using the fitted trendlines of force versus distance, it is possible to predict how deep to dig for a given force and flexibility. Figure 3-7 shows the measured average depths of the diggers for a variety of flexibilities when the maximum digging force is 0.5 N. Once again, for the same amount of input force, the more flexible diggers on average achieve a greater depth into the substrate.

These results enable design of efficient, small-scale digging systems based on the flexibility of the digger. These flexible diggers might not take the most direct path, but they will take a path that is more efficient in reaching the same depth. This passive avoidance of areas of high force is an advantage of small-scale diggers and demonstrates how the mechanics of digging change when the digger is much smaller than the grain size.

3.2 Analysis of Observed Variability in Experiments

The experiments all showed a significant amount of variability in the data. Within each trial, there was considerable scatter in the force data as the digger progressed through the substrate, as seen in Figure 3-2. However, variability in the force data

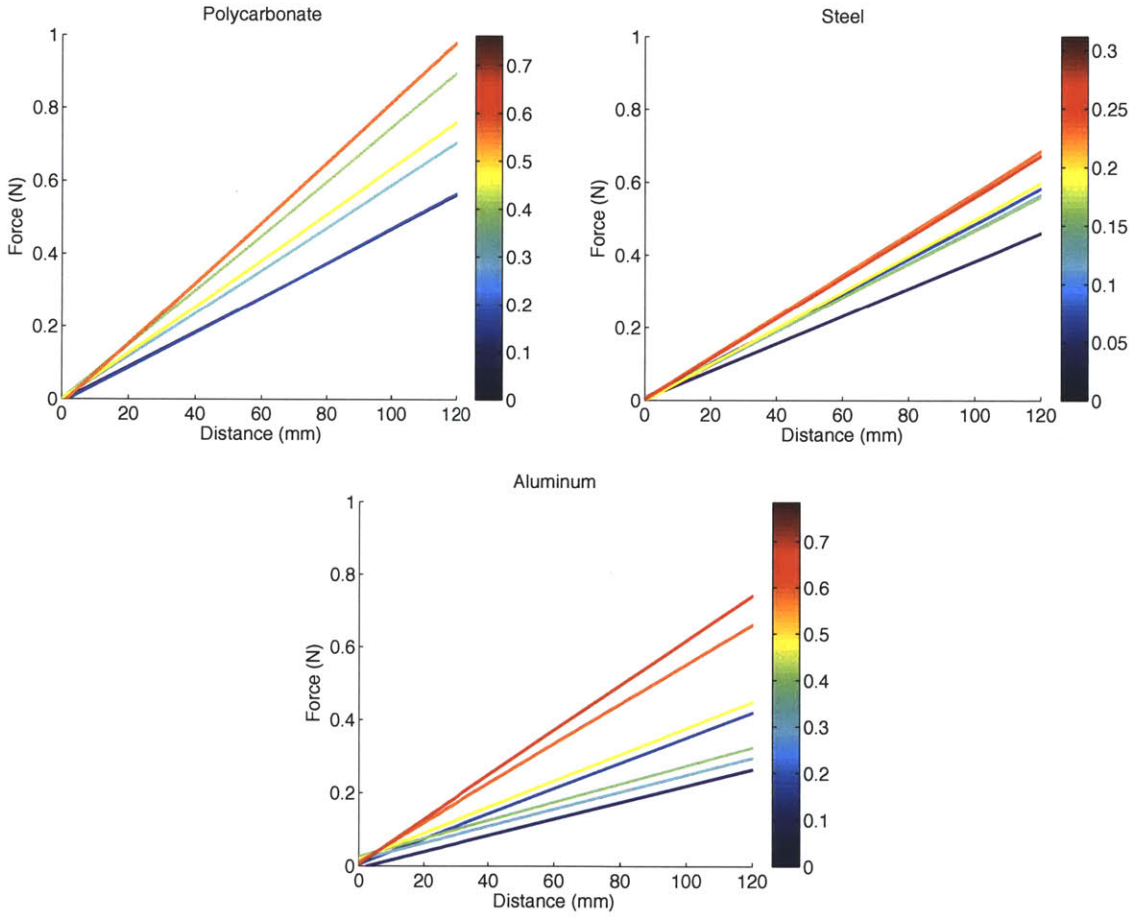

Figure 3-5: Linear fit to results for all aluminum, polycarbonate, and steel diggers. Note that decreased digger thickness (increased flexibility) leads to decreased force required to dig to a specified depth, and therefore less energy required for digging. The color bars indicate digger thickness in mm.

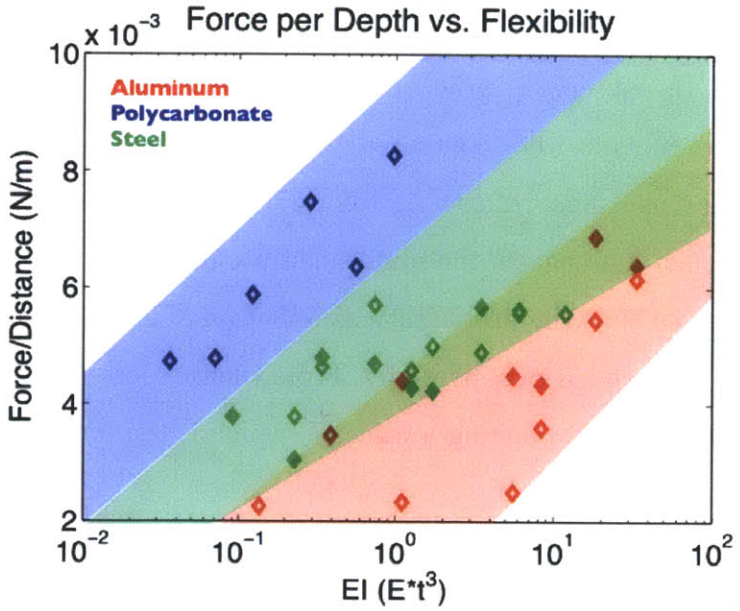

Figure 3-6: Plot of the slope of the linear fit lines for all parameters versus the flexibility of the diggers. Diggers are coded by color: blue is polycarbonate, red is aluminum, green in steel. All of the materials show the same trend: increasing flexibility can decrease the energy required for digging by more than 50%. The fill of the points indicates different grain diameters of the experiments.

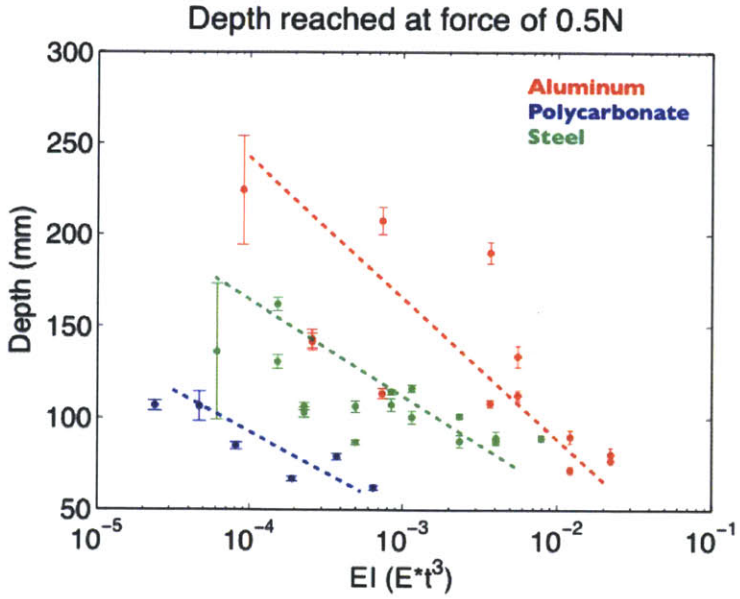

Figure 3-7: Measured average depth of diggers versus flexibility for a maximum digging force of 0.5 N. The size of the data point corresponds to the grain diameter of the experiment.

was expected because of the variability of forces inside the granular substrate.

To verify that the observed variation was due to inhomogeneity in the granular substrate, the experiments were compared to data in the literature on force distributions in granular packings. Mueth et. al. [57] analyzed the force distribution in packings of soda glass lime beads, the same substrate used for the experiments in this thesis. They observed that the probability distribution of forces in the packing above the average packing declined exponentially. From their experiments, they found that the probability, P, of a grain having a force, f, which is the force normalized by the average force, is

$$P(f) = 3(1 - 0.75e^{-f^2})e^{-1.5f} \tag{3.1}$$

which shows an exponential decay with a correction factor for probability values less than the average force. However, this model can not be directly applied to the results of the digging experiments because Mueth et. al. studied the force statistics of single grains; in our case, hundreds of grains act on the digger. Therefore, the Mueth model must be modified before comparing the variability in my experiments.

As a first order approximation, we will neglect the low force correction and focus on the exponential tail. First of all, a standard normalized exponential distribution function is of the form

$$P_{exp}(f) = \frac{1}{\beta}e^{-f/\beta} \tag{3.2}$$

when $f \geq 0$. It is known that the Erlang distribution (a particular form of the Gamma distribution) is the sum of exponential distributions [10]. This can be shown as follows. First, the Erlang distribution is given by

$$P_{Erlang}(f;\alpha,\beta) = \frac{f^{\alpha-1}}{\beta^{\alpha}\Gamma(\alpha)}e^{-f/\beta} \tag{3.3}$$

where the parameter Γ is defined as

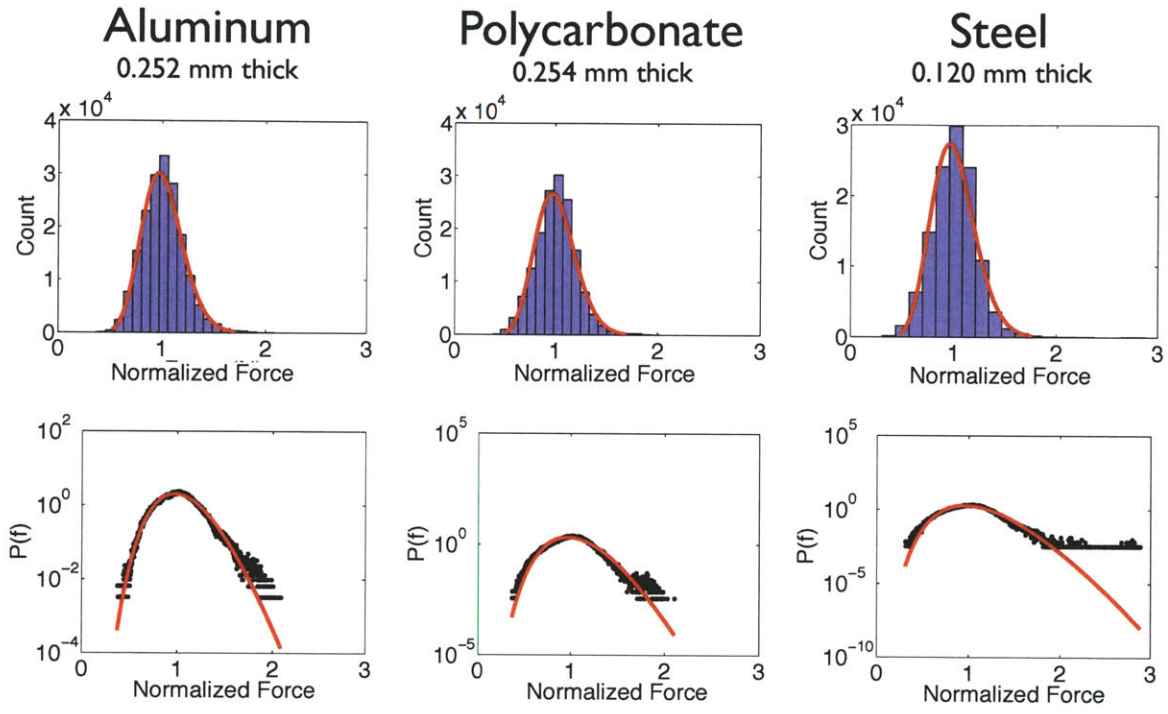

Figure 3-8: Top row are histograms of force experienced by digger in a granular substrate, overlaid with fitted Gamma distributions. Bottom row are probability density functions also fit with Gamma distributions.

$$\Gamma(\alpha) = \int_1^\infty f^{\alpha-1} e^{-f}\, df. \tag{3.4}$$

In the Erlang distribution, the parameter α can represent the number of added distributions of exponential form that were summed together to create the Erlang distribution. This can be seen when α is set to 1. The resulting distribution is

$$P_{Erlang}(f; 1, \beta) = \frac{f^0}{\beta^1 \Gamma(1)} e^{-f/\beta} \tag{3.5}$$

which equals a single exponential distribution with parameter β:

$$P_{Erlang}(f; 1, \beta) = \frac{1}{\beta} e^{-f/\beta} = P_{exp}. \tag{3.6}$$

Therefore, we expect the form of the distribution from the experimental data to be well-fit by a Erlang or Gamma distribution. Each data series was normalized by depth and then fit with a Gamma distribution. All datasets were well matched by the Gamma distribution. An example of the fit from each digger material is shown in Figure 3-8.

Therefore, the variability observed in these experiments is consistent with the force variations normally found in granular packings when the distribution of forces is as predicted from single-grain statistics.

3.3 Numerical Model of Digging

In order to further understand the mechanics of digging in granular substrates with flexible diggers, a numerical model of digging was created to test the hypothesis that increased mechanical flexibility leads to increased energy savings.

First, a series of force distributions were created for each depth in the granular system. As the average force increased, so did the standard deviation, similar to the experimental results (see Figure 3-9). Also, the digger was assigned a bending force value; this bending force is a critical force that causes the digger to deflect more than one grain diameter. This force was low for more flexible diggers and high for stiffer

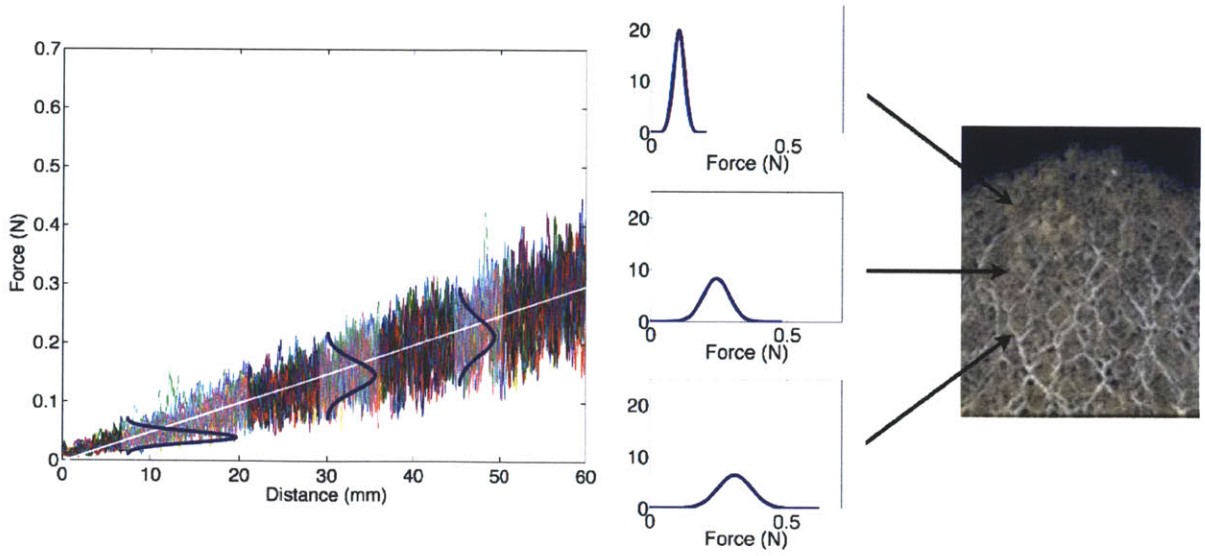

Figure 3-9: The average force distribution at increasing depths into the granular substrate. Three representative depths are shown with their corresponding force distributions. Note that as the average force increases, the standard deviation also increases. This will result in an increasing variability of force at higher depths, similar to what is observed in experiments, as shown on the left side of the figure.

diggers. Then an iterative program was created to simulate digging. At the current depth, a force value was chosen from the force distribution at that depth. That force was compared to the bending force value for the digger. If the chosen force value was less than the bending force of the digger, the chosen force value was recorded and the digging energy incremented by that force times the distance step. Then the depth was incremented by the distance step and the process was repeated. However, if the chosen force was greater than the bending force of the digger, the digger would already have bent before the system reached that force. Therefore, the chosen force was replaced by the bending force and the energy was incremented by the bending force multiplied by the distance step, multiplied by a prefactor, α. Then the process was repeated, but without increasing the depth (because the digger bent at that location, so it would have to determine if it could advance at this new location based on the force probability at that depth again). Figure 3-9 shows the force distributions at increasing depths in the substrate.

The simulations were run numerous times. Linear fits were used to compare

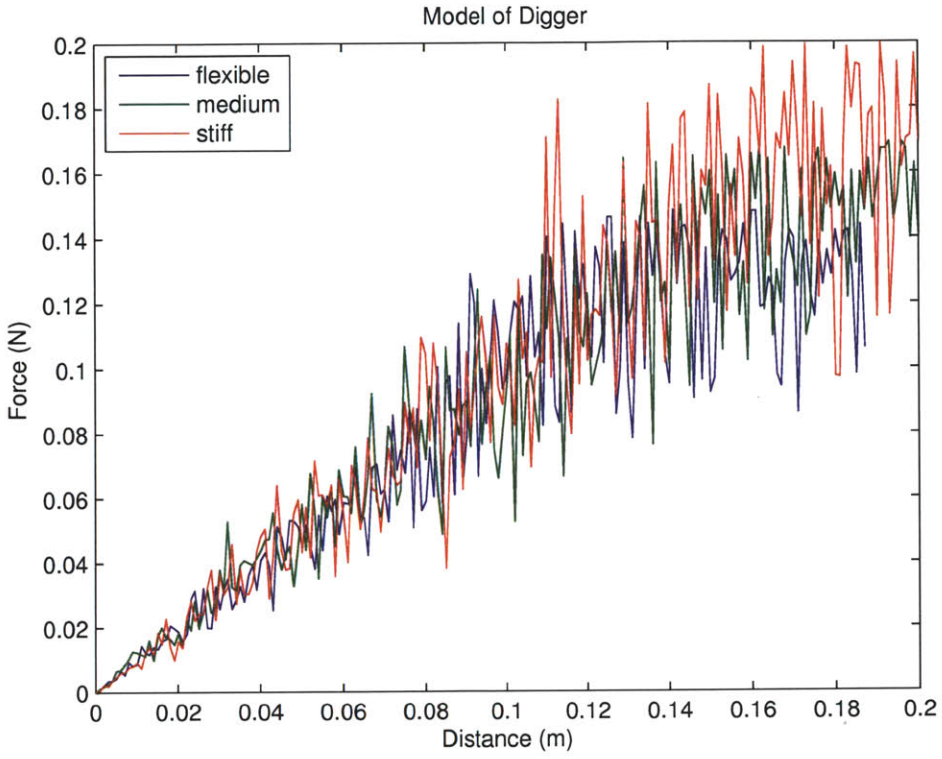

Figure 3-10: Force versus depth plot as created by the numerical model for three different stiffnesses of diggers. Note the qualitative similarities between the simulated data and the actual data, such as in Figure 3-2. In this figure, the bending force values were 0.15 N, 0.17 N, and 0.2 N in order of increasing stiffness and α was 0.01.

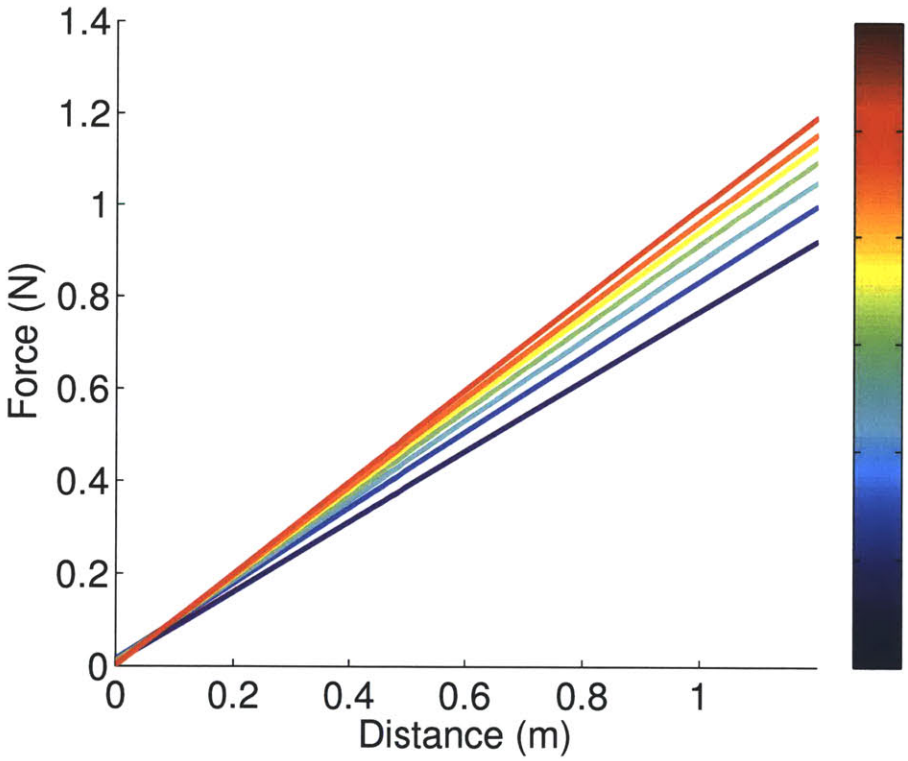

Figure 3-11: Linear fits are used to compare the results diggers with different bending forces. The color bar indicates the bending force, from high (red) to low (blue). For this Figure, the bending forces used in the model were 0.1 N, 0.26 N, 0.28 N, 0.3 N, 0.32 N, 0.34 N, 0.4 N in order of increasing stiffness.

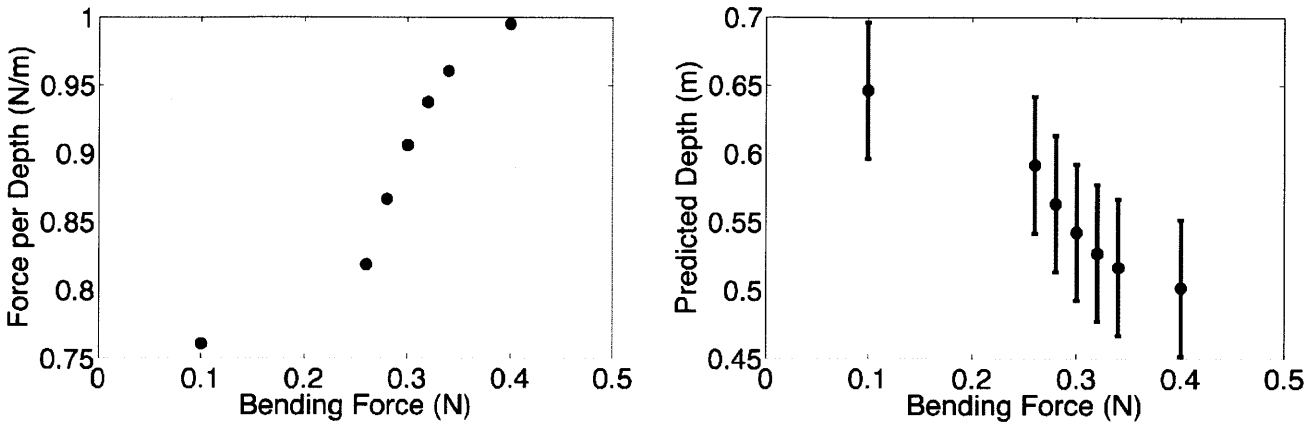

Figure 3-12: Ten simulations at each of seven different bending forces were compared. Low values of bending force correspond to high flexibility. In the plot on the left, the values of force per depth decreases with increasing flexibility (decreasing bending force). In the plot on the right, the predicted depth reached by the diggers when 0.5 N of force is applied is plotted versus the bending force. For the same input force, the more flexible diggers achieve greater depths. This is consistent with experimental results.

diggers with different bending forces and plotted together, similar to Figure 3-5. The more flexible diggers were able use less energy to reach the same depth relative to the more rigid diggers. An example plot of the simulation is shown in Figure 3-10. The plot of force versus depth looks very similar to the results from the experiments, with variation in force surrounding the average force increasing with increasing depth. At very low forces, well below the forces required for bending for these diggers, the force plots appear similar for each of the different flexibilities. That is because at these low forces, all of the diggers are stiff compared to the forces in the substrate. When the trend lines from multiple bending forces are plotted together as shown in Figure 3-11, it is clear that the more flexible diggers require less energy to reach the same depth as the stiffer diggers. Additionally, the model was used to calculate plots of force per depth versus flexibility (similar to the experimental Figure 3-6) and predicted digging depth for a given force versus flexibility (similar to the experimental Figure 3-7), as shown in Figure 3-12. All of these are similar to the results observed in the experiments: increasing flexibility leads to lower digging energy.

This simulation could also be used by designers and engineers to test new flexible

digger designs. The designers could optimize their designs to have the maximum amount of flexibility to decrease the energy required to dig, but not be so flexible that they bend very shallowly in the substrate and never reach the required depth. This sort of optimization is especially successful using numerical tools due to the variation in the individual experiments.

3.4 Experimental Investigation of Actuated Flexible Intruders in Granular Packings

In addition to the flexibility of the root path observed in the plant experiments, the reorientation of the root tip appeared to play an important role in the roots' ability to grow in granular packings and find a path of lesser resistance. Without this reorientation, the tip could get stuck in a direction that was not favorable. By adding actuation to the diggers described in the previous section, the effect of actuation on the energy of digging was investigated.

In order to test the digging energy of diggers with an actuated tip, flexible polycarbonate diggers were modified to have their tips move back and forth. This motion was created by two nitinol wires from Flexinol [26] glued to either side of the tip of the digger. The 35 mm nitinol wires contract when heated resistively. A circuit was built to provide two square waves with 25% duty cycle, 180 degrees out of phase, so that the tip would move smoothly from side to side. The circuit diagram is shown in Figure 3-13. The polycarbonate diggers were selected for these tests because they are not electrically conductive and would not lead to short circuits, unlike the aluminum or steel diggers. A summary of the diggers' thicknesses can be found in Table 3.2.

After gluing the nitinol wires to the tips of the diggers with superglue, the diggers were tested using the same method as described in the previous section. In the first set of tests, the diggers were not actuated. These results were the baseline for the actuated tests. In the second set of tests, the diggers were actuated via the flipping circuit in Figure 3-13. The actuated tests were run at 0.25 mm/s so that the frequency

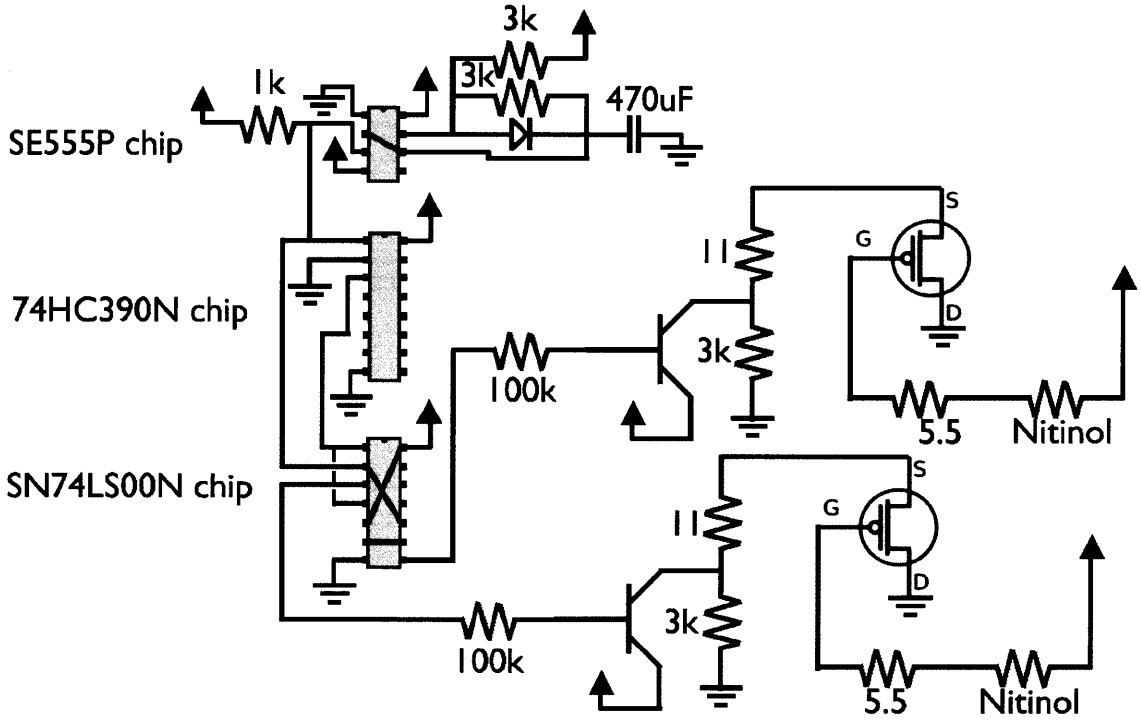

Figure 3-13: Circuit diagram for the actuated diggers. The circuit was powered with 5 V, 0.7 A from an HP E3610A DC power supply.

Table 3.2: Actuated Digger Thicknesses in mm

Polycarbonate
0.318
0.381
0.508
0.635
0.762

of flipping was faster than the time it took to travel more than one grain diameter downward. This frequency was chosen based on the speed of the observed biological motion versus the plant root growth rate. By completing one cycle during a downward displacement of one grain, the digger was able to sample more horizontal space during digging.

Results of Experimental Investigation of Actuated Flexible Intruders in Granular Packings

The actuated trials showed a distinct difference from the un-actuated trials. As shown in the representative example in Figure 3-14, the digging force repeatedly spiked sharply downward. These downward spikes corresponded to the time when the digging tip began to move in the opposite direction. This indicates that the hypothesis that the tip motion allows the diggers to find an area of lower force could be correct.

For each of the actuated diggers, the energy required for digging was calculated by averaging all of the trials of the same parameter set together and then integrating the force over the distance for both the control and actuated tests. The results are shown in Figure 3-15. In each of the tests, the energy required for digging is lower for the actuated tests than for the control tests. Note that these results do not take into account the energy required for the actuation, only for the downward motion. Therefore, the actual energy required for the actuated tests is higher than reported in Figure 3-15.

The energy expended in creating the flipping motion was calculated and taken

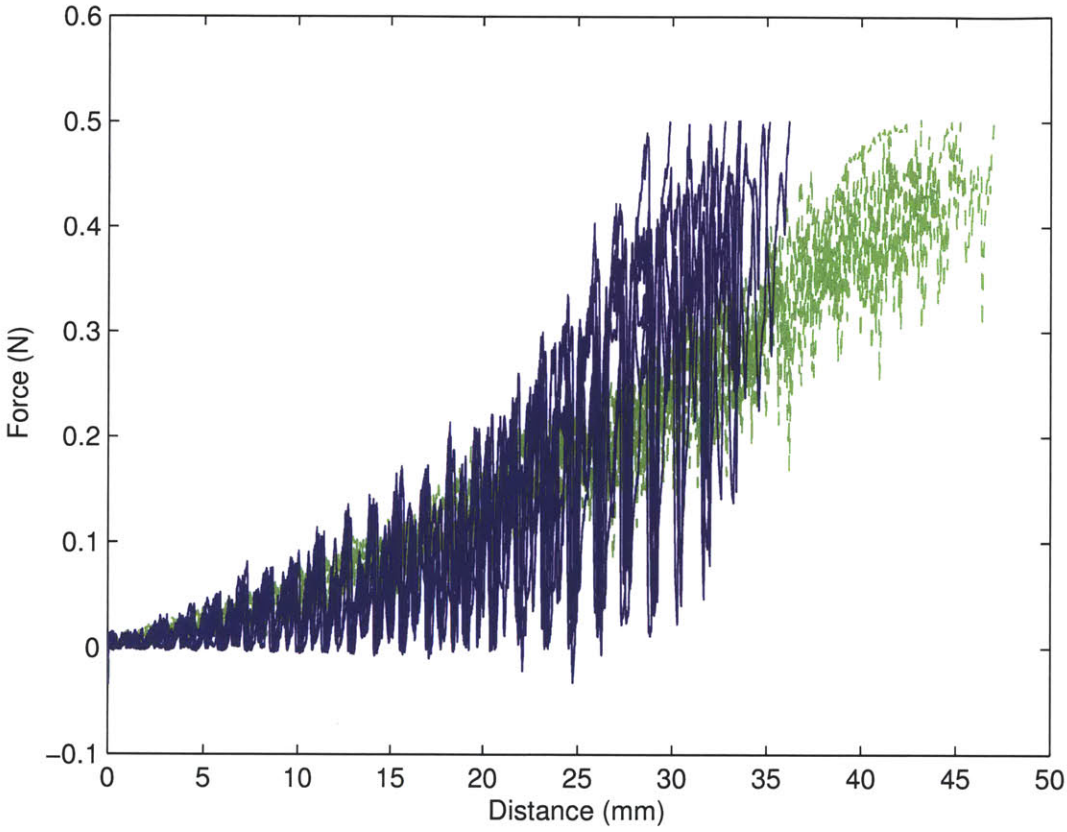

Figure 3-14: Results for digger thickness 0.381mm, actuated trials in blue, control trials in green. Note the sharp downward spikes in the actuation trials corresponding to the time when the digging tip began to move in the opposite direction.

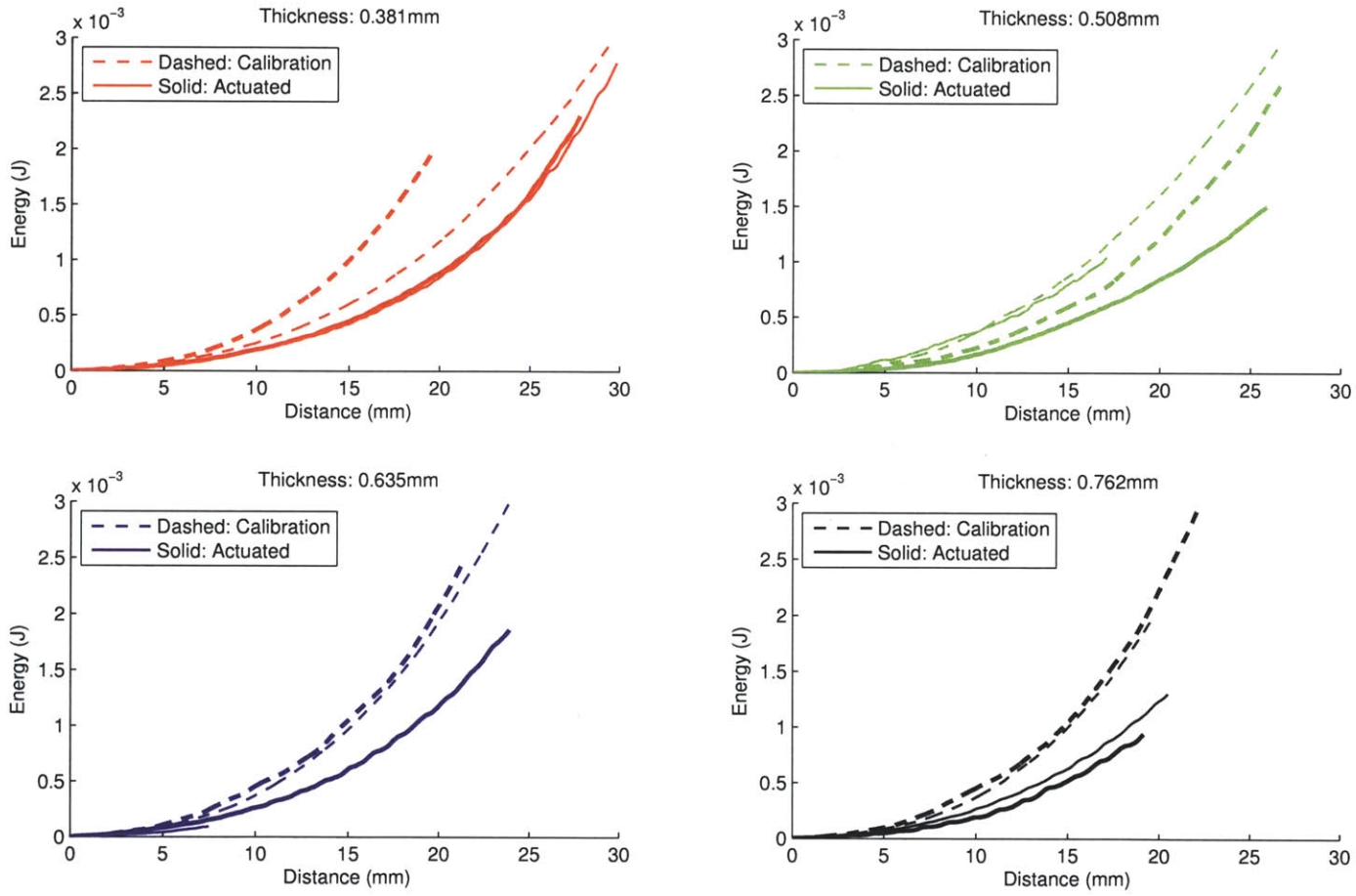

Figure 3-15: Average energy results for all trials. Each subplot is a different digger thickness. The line weight indicates the grain size; thin lines are tests in 1mm diameter grains, thick lines are 2mm diameter grains. Note that all actuated tests require less energy than the control tests.

into account. For each cycle of the actuated digger, the nitinol wire was powered for 2 seconds at 5 V and 0.7 A. (It was powered for 1 second in one direction, 1 second of no power, 1 second in the other direction, and a final 1 second off for each cycle.) The actuated tests were run at 0.25 mm/sec, so for every millimeter that the digger travelled downward, the digger expended 7 J in changing tip orientation. This amount of energy dwarfs the energy required for digging in either the actuated or control tests.

Investigating the effect of mechanical flexibility on actuated digging, it is clear that tip reorientation can also improve the energy efficiency of digging. However, this actuation is not as energy-efficient as mechanical flexibility alone if the energy cost of creating the tip reorientation is too high. This work gives a clear design parameter for the energy maximum for the tip reorientation design. Based on this research, each cycle of tip reorientation must take less than 2.5×10^{-5} J/mm to be more efficient at digging than passive mechanical flexibility.

3.5 Conclusions on Mechanical Digging Via Two Biologically-Inspired Motions

This chapter has introduced a biological digging system, plant roots, analyzed the growth of these plant roots, and investigated two digging mechanisms inspired by the plant roots: flexibility and tip reorientation. Experimental investigations of these two mechanical techniques have shown that increased mechanical flexibility can lead to a decrease in digging energy of more than 50% when the bending modulus is decreased by an order of magnitude. The variability observed in the data can be attributed to the non-homogeneous forces in the granular substrate and is consistent with previous work on force distributions in granular packings. Also, a simple numerical simulation demonstrates that the increase in digging efficiency can be attributed to the flexibility of the digger.

However, experiments with diggers whose tip orientation cycled from side to side

showed that is more energy-efficient to dig with mechanical flexibility and this active tip only if the energy used to create the changing tip orientation is less than 2.5×10^{-5} J per mm dug. Otherwise the energy used to create the changing orientation will overshadow the digging energy savings.

Chapter 4

Investigation of MEMS Technology for Digging Applications

MEMS technologies are already in widespread use. Consumer electronics, manufacturing systems, energy technologies and many other areas have made use of their small footprint and new capabilities [30, 76]. However at this time, MEMS have not been used extensively in digging technologies. Designing for MEMS actuators requires accurate knowledge of the system requirements, however when digging in granular materials, many of the models are empirical and make assumptions about the homogeneity of the substrate. However, a comparison of the size of MEMS actuators to sand grain sizes will show that these two numbers are often on a similar scale or the MEMS system is significantly smaller than the grain size, so a continuum model is not reasonable. For example, to build the flexible diggers described in the previous chapter, actuators that are smaller than the grain size would be necessary in order to build flexible-digger style robots.

This chapter develops a simple model to estimate the energy required to dig through a granular substrate. A discrete model for systems where the digger is smaller than the grain size is combined with a continuum model for systems where the digger is larger than the grain size. Using the combined model, current digging technologies are analyzed and a Matlab tool is created for use in design of digging systems that quickly and easily identifies promising technologies based on current

MEMS technology specifications.

4.1 Modeling Digging Energy

To model the energy required to dig in a granular substrate, consider two extreme cases. In the first case, the digger is much larger than the grain size. This is similar to a beach umbrella in the sand. When the pointed end of the umbrella is pushed into the sand, it is much larger in diameter than the grains of sand surrounding it. Therefore, the differences between the individual grains of sand are small and the sand can be considered using continuum approaches. Now consider the second case in which the digger is much smaller than the grain. Imagine an ant digging through a jar of marbles. In this case, the digger is much smaller than the grains and the substrate can no longer be considered homogeneous. Each of these cases is modeled separately, and then extrapolated to the scale where the digger diameter is close to the grain diameter.

4.1.1 Continuum Digging Energy Model

The continuum digging energy model assumes that the granular substrate can be modeled as homogeneous at size scales where the digger is much larger than the grain size. For this case, the energy required for the digger to traverse the media is simple. Energy is force times distance. We assume that the force in the system is a hydrostatic force, F_N, due to the semi-infinite extent of the substrate, and that the digger will move its body diameter, $2r$, where r is the radius of the digger (assuming a cylindrical digger.) Therefore, the energy, E, required is

$$E = F_N 2r. \tag{4.1}$$

In this case, the frictional energy along the body of the digger is neglected and can generally be minimized through design choices in the construction of the digger. Observations from the flexible digger experiments showed that the largest amount

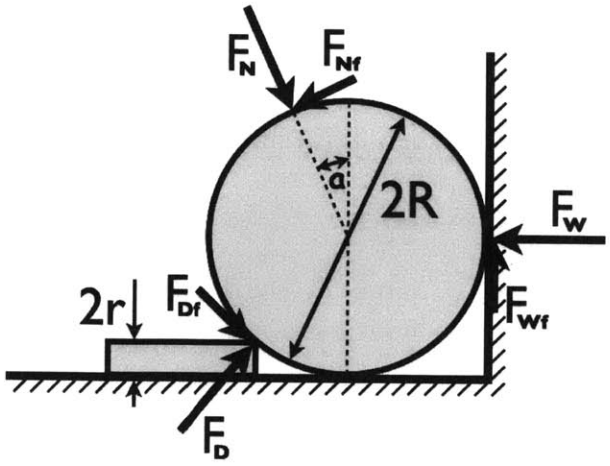

Figure 4-1: Schematic of static grain and relavent notation.

of energy was used to rearrange the grains near the tip of the digger and the frictional energy was an order of magnitude lower because it only involved minor grain rearrangements.

4.1.2 Discrete Digging Energy Model

The discrete digging energy model assumes that the size of the digger is much smaller than the diameter of the grains. In this regime, consider a simple two-dimensional system with geometric constraints and an applied force that is a resultant of all forces acting on the grain from the system. A diagram of the system is in Figure 4-1.

The grain has a radius R and the digger has a radius r. All contacts have friction of value μ. The force from the digger acting on the grain is F_D, the force from the constraint wall is F_W, and the forces from the system can be combined into a resultant force, F_N. The angle that the system force, F_N, is acting with respect to the vertical is α. The digger is constrained to move only in the horizontal direction (as shown by the wall at the bottom of the system, however, there is no friction between the horizontal wall and the digger; it is only a geometric constraint). Assuming that we know the system force and its direction, F_N and α, the friction μ, and the radii of the grain and the digger, R and r, we solve for the reaction forces F_W and F_D from

equilibrium. The equilibrium equations are

$$\sum F_x = -F_W + F_N \sin\alpha + F_D \sin\beta - F_N\mu\cos\alpha + F_D\mu\cos\beta \tag{4.2}$$

$$\sum F_y = F_W\mu - F_N \cos\alpha + F_D \cos\beta - F_N\mu\sin\alpha - F_D\mu\sin\beta \tag{4.3}$$

$$\sum M_z = \mu(F_W + F_N + F_D), \tag{4.4}$$

where β is a geometric parameter defined as

$$\beta = \sin^{-1}\left(\frac{2\sqrt{r(R-r)} - x}{R}\right). \tag{4.5}$$

To calculate the energy the digger must expend to dig under the grain, we integrate in x from the point where the digger first touches the grain to the point when the digger is underneath the mid-point of the grain. This length of integration is $2\sqrt{r(R-r)}$ by geometry. The energy used by the digger to move the grain is

$$E = 2F_N\cos\alpha\left(R + \mu\sqrt{r(R-r)} - r\right). \tag{4.6}$$

This energy is dependent on the orientation and magnitude of the resultant force of the system on the grain, α and F_N. From Eq. 4.6, it is clear that the energy is maximum when α is 0. Therefore,$\cos\alpha$ is replaced with 1 in all future equations to compute an upper bound on the energy.

To better understand the impact of size scale on digging energy, the energy equation is non-dimensionalized to

$$\hat{E} = 2\left(1 + \mu\sqrt{\hat{r} - \hat{r}^2} - \hat{r}\right) \tag{4.7}$$

where the two non-dimensional parameters, $\hat{E}$ (a dimensionless energy) and $\hat{r}$ (the dimensionless digger size) are defined as

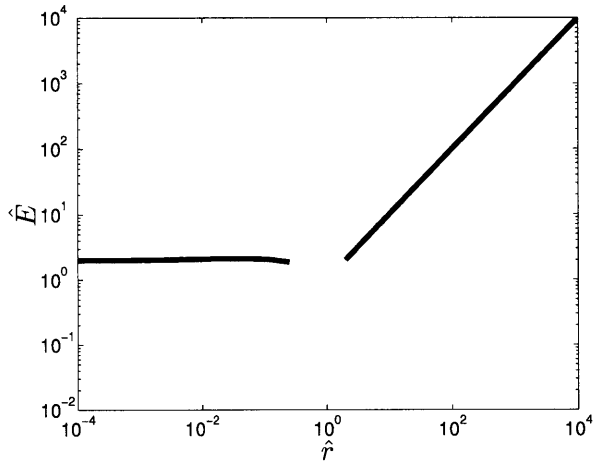

Figure 4-2: Non-dimensional energy requirement for digging at a variety of size scales. The left portion of the line is from the discrete energy analysis with a μ value of 0.4 and the right portion of the line is from the continuum energy analysis.

$$\hat{E} = \frac{E}{F_N R} \tag{4.8}$$

$$\hat{r} = \frac{r}{R} \tag{4.9}$$

4.1.3 Combined Multi-Scale Model Using Non-Dimensional Parameters

In order to compare the continuum digging energy to the discrete digging energy, we rewrite Eq. 4.1 in terms of $\hat{E}$ and $\hat{r}$, which becomes

$$\hat{E} = 2\hat{r}. \tag{4.10}$$

Now using the non-dimensional equations from Eqns. 4.7 and 4.10, we plot both the continuum and the discrete digging energy in Figure 4-2. The plot shows our estimate for the energy necessary to dig in granular materials over eight orders of magnitude, from situations where the digger is much smaller than the grain size to scenarios where the digger is much larger than the grain size.

4.2 Using The Multi-Scale Model To Select MEMS Actuator Technology

The plot in Figure 4-2 shows the required energy for digging over a wide range of size scales, from a digger that is much larger than the grain size to a digger that is much smaller than the grain size. This plot can also be used to graphically analyze different actuator technologies and evaluate their suitability for a given digging application.

For this analysis, the summary of actuator technologies from a MEMS review paper [7] is used. Other actuator technologies can be added to this list and analyzed in the same way. The digger radius is assumed to be ten times the actuator size to account for any additional mechanisms and power storage that is needed inside the digger. The grain size and the substrate characteristics of confining pressure and friction angle are user-specified for a given application. From these assumptions and values, the data from [7] can be rewritten in terms of the non-dimensional parameters $\hat{E}$ and $\hat{r}$. Overlaying these results on the energy requirement plot shows which technologies hold the most design potential for the specified digging application. As shown in Figure 4-3, any actuator whose energy area is above the requirement line should be further investigated for digging designs.

It should be noted that plotting the actuators on the energy requirements plot requires knowledge of the system for which you are designing the digger. The grain size and confining pressure of the formation need to be specified in order to accurately calculate the non-dimensional values $\hat{E}$ and $\hat{r}$. For example, if the grain size used in Figure 4-3 was increased by ten times, then the actuator technologies would map to different parts of the plot based on the changed ratio between actuator size and grain size. Therefore, a graphical user interface (GUI) was developed to aid in the design process, as shown in Figure 4-4. The Matlab code for the GUI is included in Appendix C.

The GUI allows the user to specify parameters of the granular substrate, including the coefficient of friction, the confining pressure of the soil, and the radius of the grains. Using the continuum and discrete models and the MEMS actuator database,

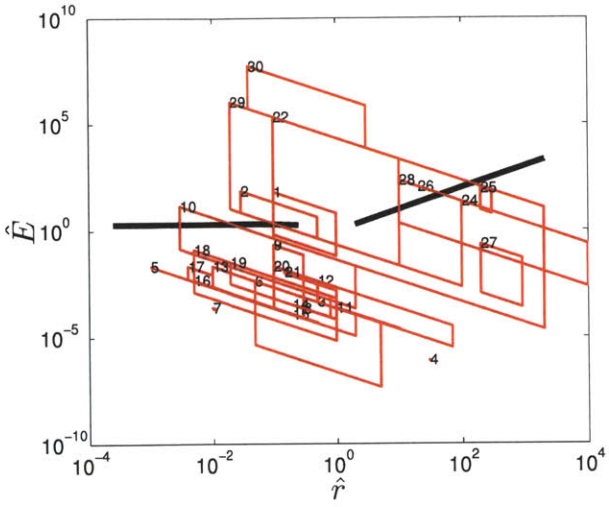

Figure 4-3: Digging energy requirements plot overlaid with MEMS actuator technologies energy outputs. Each actuator is referred to by number from Figure 4-4. Plot created with grain radius of 0.1 mm, coefficient of friction of 0.3, and confining pressure of 14 MPa.

along with the user inputs, the GUI outputs the digging energy requirements plot with an overlay of the MEMS actuators energy outputs.

This analysis tool gives designers of digging robots a new and quick way to compare their system requirements against a large variety of actuators. By referencing a large database of actuators, this tool can help designers quickly narrow their search to actuators that will be most effective for their applications, without having to do tedious calculations by hand. Also, keeping all the actuator data in a database allows for quick updates and additions of new actuator data, so the tool can evolve along with technology to always have accurate and relevant information for actuator selection.

This tool was specifically created for the selection of actuators for digging applications over a wide range of size scales. By bridging the gap from traditional actuator sizes and technology to MEMS technologies and smaller-scale devices, this tool gives designers a way to quickly identify technologies to investigate further for their application, especially in new MEMS areas where the designers may not have as much experience.

Also, this graphical method of representing the design space is a new and easy

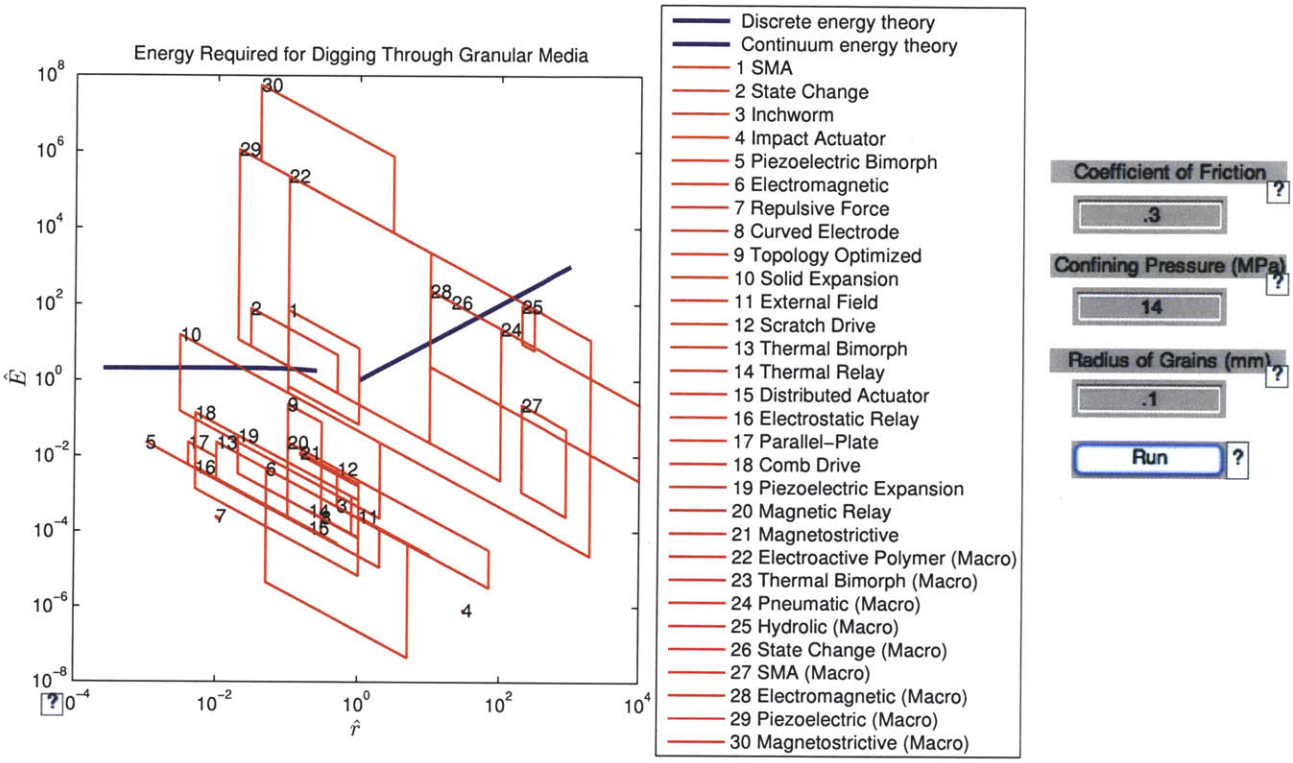

Figure 4-4: Actuator technology overlaid on energy requirements plot in a graphical user interface (GUI) that allows for user-specification of the properties of the substrate that the digger is being designed for. Friction angle, confining pressure in the formation, and grain size are user inputs (in this plot the parameters are grain radius of 0.1 mm, coefficient of friction of 0.3, and confining pressure of 14 MPa.) The plot of energy requirements and actuators technologies are then automatically calculated and plotted.

way to visualize design choices and tradeoffs. For example, in Figure 4-4, the designer could quickly see that the actuator technologies of electroactive polymers, piezoelectrics, and magnetostrictive actuators could work well for this application, depending on the desired digger size. However, magnetostrictive actuators would give a larger margin of error. Electromagnetic actuators would be more likely to work at larger size scales. Solid expansion designs could only work at smaller scales. These sorts of tradeoffs are easily seen and understood through this graphical representation of the design space.

This new MEMS design tool, along with the discrete and continuum analyses of the energetics of digging through granular materials, gives designers a way to quickly identify promising MEMS actuation technologies for use in granular digging applications. The MEMS GUI, in combination with the information about the energy advantages of flexible diggers from the previous chapter, gives designers of robotic diggers new methods of digging and new methods of sizing actuators for the new flexible robotic diggers.

Chapter 5

Discussion and Outlook

This thesis uses inspiration from biology to investigate digging systems where the diggers are smaller the the grain size of the granular substrate. First, plant root growth was investigated as a model system for digging robots. The pinto beans were an excellent experimental subject because they were slow growing and lacked a nervous system so their control algorithms were simple. The results of this research do not appear surprising at first glance: plant roots are sensitive to the forces in the granular substrate and the roots grow stronger over time. However, there are some subtleties in the results that require more focus. The increase in strength over time was not accompanied by a measurable increase in root diameter. When the roots are growing, the digging force is created by the cellular osmotic pressure. In order to significantly increase the force exerted by the roots, the diameter should change accordingly but this was not observed in these experiments. This increase in force without associated geometric changes should be studied in more detail. Additionally, the tip motion of the roots was noted in all experiments. Other researchers are investigating potential mechanical motivations of this motion, such as giving increased torque when encountering an obstacle in the soil. It would be interesting to tie together the quantitative measurement techniques that I have used in these experiments with more realistic agricultural scenarios to try to understand the biological motivation. Perhaps avoidance of high-force areas is not the only use of the tip motion during plant growth.

After characterizing the abilities of pinto bean roots using a photo-elastic growing

system, two elements of the roots where further explored using mechanical engineering experiments: flexibility and tip reorientation. It was found that increasing the mechanical flexibility of the digger by an order of magnitude when the diggers are smaller than the grain size can lead to energy savings of more than 50%. There is large variability in the experimental data but this variability is consistent with the force fluctuations normally found in granular materials. The variability was well-fit by a Gamma distribution, which is as expected since the probability density functions of the force on individual grains is exponential. Additionally, a numerical model of digging showed that the increased flexibility of the digger could allow it to "sample" more configurations when it encountered an area of high force, which would give the more flexible diggers a greater chance of finding a path with lesser resisting force. Active tip reorientation can also help a digger find paths of lesser resistance, however, the tip reorientation is more energetically costly than the simple mechanical flexibility if the energy used to create the reorientation is more than 2.5×10^{-5} J per mm dug. In plant root growth, either plants are able to create this reorientation motion using very little energy or the motion is related to some other biological function like sensing for nutrients and not responsible for digging energy efficiency.

These results are very exciting for mechanical diggers. By using less traditional mechanisms for digging, it is possible to accomplish large energy savings in the regime where the digger is smaller than the grains. The caveat is whether it is important how far away from the starting point the end is, or where exactly the endpoint is. These sorts of flexible diggers might require less energy to achieve a certain depth, but due to their flexible nature, the exact location at that depth-plane is not specified. The tradeoff with energy savings is an imprecision with location. For fields such as exploration, this could be a benefit. From the same starting point, these small-scale flexible diggers could go father than traditional rigid diggers and also have some inherent variability in their final locations. Also, the energy savings would result in further travel for the same battery size compared to more rigid diggers.

Future work on flexible diggers should focus on increasing their autonomy. Small-scale batteries, flexible power systems, and flexible actuation techniques all have to

be implemented to be able to fully harness the energy savings of flexible digging. One way to source MEMS technologies that would be appropriate for flexible digging would be to use the Matlab MEMS selection tool created in this thesis. By comparing the scale of the digger to the grain size, the selection tool would allow designers to quickly focus in on actuators with the necessary specifications. In the future, the energy savings associated with flexibility could be mapped onto the same chart. This could fully capture the tradeoffs in digging designs, including the limitations in depth exhibited by extremely flexible diggers and the energy cost of a variety of digging flexibilities. This opens a new paradigm of energy-efficient digging techniques based on the force-chain avoidance exhibited by plant roots.

Appendix A

Pumping Granular Materials Constrained By Flexible Boundaries

This appendix describes another system where the granularity of the substrate affects the dynamics: the small intestine.

Biologists have observed two primary motions in the human small intestine: peristalsis and segmentation [46, 72]. These two motions are closely related to two common mechanical pumps: peristaltic pumps and impedance pumps. Both of these mechanical systems have undergone extensive analysis and experimentation for mechanical applications with Newtonian fluids. However, medical literature notes the presence of particulate matter as well as the non-Newtonian behavior of digesta [42, 43, 46, 72]. None of the previous experiments test what happens in the systems when high concentrations of particles are added to the fluids.

Therefore, to understand how the small intestine is able to transport complex materials through its length, peristaltic pumping was investigated experimentally to compare the pumping characteristics of systems with high-volume-fractions of grains to systems pumping pure Newtonian fluids.

A.1 Peristaltic Pumping

A.1.1 Background of Peristalsis

Peristaltic pumping of Newtonian fluid was investigated by Shapiro in 1969 [63]. He calculated the fluid flow patterns inside a tube undergoing peristaltic pumping and confirmed his theory experimentally. He noted two interesting phenomena: a "reflux" area at the edge of the tube and "trapping" in the center of the tube. Further work by other researchers expanded the theory of peristaltic pumping for a variety of conditions [12, 44, 55, 69], including non-Newtonian fluids [32] and fluids with a low concentration of neutrally-bouyant particles [36, 53, 68].

A.1.2 Experimental Investigation of Peristaltic Pumping of Granular Materials

In order to better understand the effect of peristalsis is when the transport fluid has a high concentration of grains, an apparatus was built that could create a peristaltic wave at a variety of amplitudes. The apparatus is divided into two sections: the fluid loop and the roller jig.

The fluid loop was a loop of PVC pipe with one long section of clear flexible (but inextensible) tubing. (This setup is similar to [33]). The PVC pipe was Schedule 20 and the tubing was 4 mil polypropylene, sold as 1 inch wide when flattened (so the tube has a circumference of 2 inches and an internal diameter of 0.637 inches or 16.2 mm). The polypropylene section was approximately one meter long and the sides PVC sections were 10 cm long. There was a valve at one of the PVC corners so that the system could be filled and emptied. This allowed for different viscosities of fluid to be used. All joints in the system were sealed using silicone aquarium sealant.

The roller jig had a small carriage with two rollers whose spacing could be varied (Figure A-1). This spacing was the inverse of the peristaltic wave amplitude. The carriage moved along a tract of two parallel half-inch steel rods using a lead screw powered by a DeWalt drill motor connected to a power supply. An overhead view

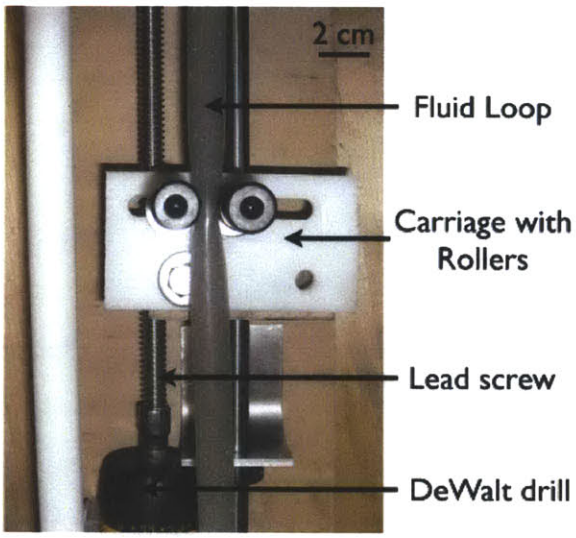

Figure A-1: The peristaltic pumping apparatus.

of the carriage and rollers when the fluid loop is in place is shown in the inset in Figure A-1.

All experiments were performed using a wave speed of 0.01 m/s so the system could be assumed to be quasi-static and quasi-steady. Soda lime glass beads of 1 mm diameter completely filled the clear section of tube but did not extend around any of the corners of the fluid loop, so they would not clog the loop. Experiments were performed for a variety of viscosities ranging from water (1 mPa·s) to glycerin (measured to be 244 mPa·s), each with different wave amplitudes. The motion of a sample of grains was recorded for each trial, some by hand and some by camera.

A.1.3 Results of Peristaltic Pumping of Granular Materials

The direction and velocity of the grains were observed to depend on the viscosity of the background fluid. For high viscosities like glycerin, the grains moved in the direction of the peristaltic wave, and the velocity of their motion was linearly related to the amplitude of the peristaltic wave. However, as the viscosity of the background fluid decreased, the magnitude of the grains' motion decreased until, at very low viscosities like water, the grains moved in the opposite direction of the peristaltic wave. These results are summarized in Figure A-2, where the compression ratio is

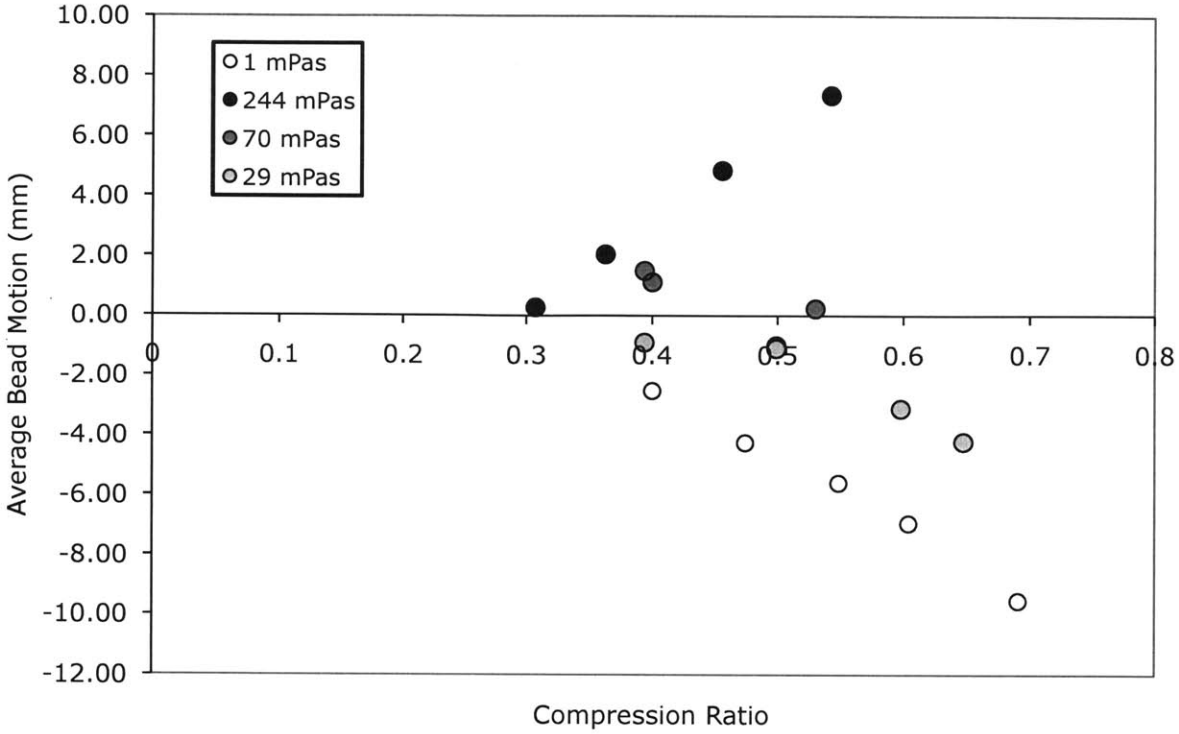

Figure A-2: The results of peristaltic pumping of granular systems. The compression ratio is the ratio between the amplitude of the wave and the radius of the tube. Therefore, a compression ratio of zero corresponds to no wave amplitude, and a compression ratio of 1 corresponds to a complete closure of the tube by the peristaltic wave.

the ratio between the amplitude of the wave and the radius of the tube. Therefore, a compression ratio of zero corresponds to no wave amplitude, and a compression ratio of one corresponds to a complete closure of the tube by the peristaltic wave.

In traditional peristaltic pumping, the material follows the direction of the peristaltic wave. However, these results show that at high volume fractions of grains, the grains move backwards relative to the peristaltic wave. This could have important implications in medical treatments that significantly alter the natural viscosity of chyme in the small intestine. If the viscosity is too low, the digesta might not flow correctly or even begin to flow backwards, leading to blockages and medical complications.

The results shown here reach a maximum compression ratio of 70%, which was based on the limitations of the apparatus. At a compression ratio of 100%, namely

with a tube that is completely occluded by the peristaltic wave, it is expected that the grains in the low-viscosity fluid would be transported in the direction of the wave. However, there is no observable change in the magnitude of reverse transport for the low-viscosity results, even at compression ratios as high as 70%.

Future work should continue to explore high-amplitude peristaltic waves and also a larger range of low-viscosity fluids to investigate the universality of the reversed flow phenomena. Since a peristaltic wave that was large enough in amplitude to occlude the tube would cause all transport to be in the direction of the wave, there should be more investigation of the limiting amplitude wave where flow reversal is observed. Additionally, preliminary work showed that the transport of the grains was very sensitive to the concentration of the grains and the reverse flow phenomena only occurred when the fraction of grains was close to the random loose packing value. Further work in this area could quantify the effect of grain volume fraction on modes of peristaltic transport. The results from this work should be taken into account by the biological community when creating treatments for the small intestine that might alter the viscosity of the chyme, especially for dietary or disease-related reasons.

Appendix B

Biological Digging Survey

Body type sketch	Phylum	Class	Family	Genus	L?A	body type	soil water content	kinematics	notes	L (mm)	r (mm)	A (mm)	bend radius R (mm)	Cite
	nemertea				>>	soft	damp	flexible		20	0.35	0.15	10	
	nematoda		leptosomatida		>>	soft	damp, wet	flexible				0.15		
	annelida	polychaeta			>>	soft	damp, wet	flexible	tube worms	1000	100	0.15	50	
	annelida	polychaeta	aphroditidae	thalenessa	>>	soft	damp	flexible	specialized for digging near wave action	40	4	0.15	10	
	annelida	polychaeta	glyceridae	glycera	>>	soft	damp, wet	flexible	dig with long proboscis	350	15	0.15	50	
	mollusca	gastropoda		oliva	>>	soft+shell	wet	combination	locomotes just beneath sand surface			0.15		
	mollusca	gastropoda		olivella	>>	soft+shell	wet	combination				0.15		
	mollusca	gastropoda		donax	>>	soft+shell	wet	combination				0.15		
	tardigrada				~	hard	damp	traditional	uses claws to move grain to grain	0.5	0.1	0.15	0.5	
	tardigrada			batillipes	~	hard	damp	combination	uses adhesive disks to move between grains	0.5	0.1	0.15	0.5	
	arthropoda	arachnida			<<	hard	dry, damp, wet	traditional	mites			0.15		
	arthropoda	crustacea	copepoda		~	?	dry, damp	?	inerstitial			0.15		

Figure B-1: Biological Survey 1.

Body type sketch	Phylum	Class	Family	Genus	L?A	body type	soil water content	kinematics	notes	L (mm)	r (mm)	A (mm)	bend radius R (mm)	Cite
	arthropoda	crustacea	copepoda	asellopsis	>	?	dry, damp	?	burrower			0.15		
	arthropoda	crustacea	decapoda	ocypode	>>	hard	dry, damp, wet	traditional	semi-permanent burrows			0.15		
	arthropoda	crustacea	decapoda	dotilla	>>	hard	dry, damp, wet	traditional	extracts organics from sand	150	50	0.15		
	arthropoda	crustacea	decapoda	ovalipes	>>	hard	dry, damp, wet	traditional	rapid burrower			0.15		
	arthropoda	crustacea	decapoda	uca	>>	hard	dry, damp, wet	traditional	fiddler-crab - muddy digger			0.15		
	arthropoda	insecta	coleoptera	bledius	>	hard	dry, damp	traditional				0.15		
	rotifera				<	hard+soft	dry	traditional				0.15		
	gastrotricha				<	soft+scales		flexible	scales/spines	0.14	0.02	0.15	0.1	
	kinorhyncha				<	hard	damp, wet	combination	spines used like rachet in sand	1	0.1	0.15	1	
	platyhelminthes				~	soft	wet	flexible	flatworms	10	1	0.15	3	
	cnidaria				<	hard+soft	dry, damp, wet	flexible	related to corals and jellyfish			0.15		

Figure B-2: Biological Survey 2.

Appendix C

Matlab Code for MEMS Actuator Design Tool

```
1
2  function energy_gui1
3  % ENERGY_GUI1 Plots the energy vs scale data for digging and
4  % allows users to select the soil parameters and then plots
5  % current digging technology over the energy curves.
6
7      %  Create and then hide the GUI as it is being constructed.
8      f = figure('Visible','off','Position',[560,600,850,585]);
9
10     %  Construct the components.
11     hfric = uicontrol('Style','text','String','Coefficient of Friction',...
12             'Position',[685,420,150,15]);
13        hfric_q = uicontrol('Style','pushbutton','String','?','Position',...
14                  [835,420,15,15]);
15
16     fric = uicontrol('Style','edit',...
17                      'Position',[685,400,100,25]);
18
19     hpres = uicontrol('Style','text','String','Confining Pressure (MPa)',...
20             'Position',[685,360,150,15]);
```

```
21        hpres_q = uicontrol('Style','pushbutton','String','?','Position',...
22                  [835,360,15,15]);
23
24     pres = uicontrol('Style','edit','Position',[685,340,100,25]);
25
26     hrad = uicontrol('Style','text','String','Radius of Grains (mm)',...
27            'Position',[685,300,150,15]);
28        hrad_q = uicontrol('Style','pushbutton','String','?','Position',...
29                  [835,300,15,15]);
30
31
32     rad = uicontrol('Style','edit','Position',[685,280,100,25]);
33
34  %   htext = uicontrol('Style','text','String','Assumptions',...
35  %          'Position',[515,200,150,15]);
36
37     hrun = uicontrol('Style','pushbutton',...
38             'String','Run','Position',[685,240,100,25],...
39             'Callback',{@runbutton_Callback});
40        hrun_q = uicontrol('Style','pushbutton','String','?','Position',...
41                  [810,240,15,25]);
42
43     ha = axes('Units','Pixels','Position',[60,100,610,385]);
44        haxes_q = uicontrol('Style','pushbutton','String','?','Position',...
45                  [40,80,15,15]);
46
47     align([hfric,hpres,hrad,hrun,fric,pres,rad],'Center','None');
48
49
50     % Initialize the GUI.
51     % Change units to normalized so components resize
52     % automatically.
53     set([f,ha,hfric,hpres,hrad],...
54     'Units','normalized');
55     %Create a plot in the axes.
56     %current_data = peaks_data;
```

```
57    %surf(current_data);
58    % Assign the GUI a name to appear in the window title.
59    set(f,'Name','Actuator Technology GUI')
60    % Move the GUI to the center of the screen.
61    movegui(f,'center')
62    % Make the GUI visible.
63    set(f,'Visible','on');
64
65    %  Callbacks for simple_gui. These callbacks automatically
66    %  have access to component handles and initialized data
67    %  because they are nested at a lower level.
68
69    %  Pop-up menu callback. Read the pop-up menu Value property
70    %  to determine which item is currently displayed and make it
71    %  the current data.
72       function popup_menu_Callback(source,eventdata)
73          % Determine the selected data set.
74          str = get(source, 'String');
75          val = get(source,'Value');
76          % Set current data to the selected data set.
77          switch str{val};
78          case 'Peaks' % User selects Peaks.
79             current_data = peaks_data;
80          case 'Membrane' % User selects Membrane.
81             current_data = membrane_data;
82          case 'Sinc' % User selects Sinc.
83             current_data = sinc_data;
84          end
85       end
86
87    % Push button callbacks. Each callback plots current_data in
88    % the specified plot type.
89
90    function surfbutton_Callback(source,eventdata)
91    % Display surf plot of the currently selected data.
92       surf(current_data);
```

```
93      end
94
95      function meshbutton_Callback(source,eventdata)
96      % Display mesh plot of the currently selected data.
97         mesh(current_data);
98      end
99
100     function contourbutton_Callback(source,eventdata)
101     % Display contour plot of the currently selected data.
102        contour(current_data);
103     end
104
105
106 % ADDING ENERGY FUNCTIONALITY
107 % ------------------------------------------------------------
108  % INSERT FUNCTIONALITY OF RUN BUTTON
109      function runbutton_Callback(source,eventdata)
110
111      %  function edittext1_Callback(hObject,eventdata)
112     mu = str2double(get(fric,'string'))
113     P = str2double(get(pres,'string'))
114       P = P*1000000  %changing pressure to Pascals
115     Rad_part = str2double(get(rad,'string'))
116       Rad_part = Rad_part/1000; %in meters
117
118
119 r = 0.25 %mm
120 r = r/1000  %m
121 R = 1     %mm
122 R = R/1000  %m
123 %mu = 0.5
124 %mu = input('Friction Coefficient: ');
125 %P = input('Confining Pressure in megapascals: ');
126
127
128 for i=10:10:10000;
```

```
129         r_hat(i/10)=(r/(R./10.*i));
130 end
131 r_hat = transpose(r_hat);
132
133 L = length(r_hat);
134
135 for i=1:L
136 e_hat(i) = 2.*(1+mu.*sqrt(r_hat(i)-(r_hat(i).*r_hat(i)))-r_hat(i));
137 end
138 e_hat = transpose(e_hat);
139
140 loglog(r_hat,e_hat,'LineWidth',2)
141 hold on
142 title('Energy Required for Digging Through Granular Media')
143 xlabel('\hat{r}','Interpreter','latex','FontSize',12)
144 ylabel('\hat{E}','Interpreter','latex','FontSize',12)
145
146 %Then we plot the digging energy required for large r_hat
147
148 for i=1:1000
149    r_hat(i) = i ;
150 end
151
152 loglog(r_hat,r_hat,'LineWidth',2)
153 hold on
154
155 % Now we add on the boxes for current actuator energies using inputs from
156 % the user for grain size
157
158 % Actuator Matrix:
159 % Min(max actuator displacement (m)), Max(max actuator displacement (m)), Min(max
160 % energy (N)), Max(max energy (N))
161
162 A = [0.00001, 0.0001, 0.03, 3  %SMA
163     0.000003, 0.00005, 0.1, 1  %State Change
164     0.00005, 0.000051, 0.0001, 0.00011  %Inchworm
```

```
165      0.003, 0.0031, 0.00001, 0.000011  %Impact Actuator
166      0.0000001, 0.0002, 0.00001, 0.00001  %Piezoelectric Biomorph
167      0.000005, 0.0005, 0.0000001, 0.0001  %Electromagnetic
168      0.000001, 0.0000011, 0.000001, 0.0000011  %Rupulsive Force
169      0.00003, 0.000031, 0.00003, 0.000031  %Curved Electrode
170      0.00001, 0.00003, 0.00001, 0.01  %Topology Optimized
171      0.0000003, 0.0002, 0.0002, 0.02  %Solid Expansion
172      0.0001, 0.001, 0.0001, 0.00011  %External Field
173      0.00005, 0.007, 0.0001, 0.001  %Scratch Drive
174      0.000001, 0.0002, 0.00001, 0.0001  %Thermal Bimorph
175      0.00002, 0.0001, 0.00003, 0.000031  %Thermal Relay
176      0.00002, 0.000021, 0.00001, 0.000011  %Distributed Actuator
177      0.0000005, 0.00005, 0.00001, 0.000011  %Electrostatic Relay
178      0.0000004, 0.000001, 0.00001, 0.00004  %Parallel-Plate
179      0.0000005, 0.0001, 0.000003, 0.0003  %Comb Drive
180      0.000002, 0.00008, 0.00003, 0.0003  %Piezoelectric Expansion
181      0.00001, 0.0001, 0.0001, 0.001  %Magnetic Relay
182      0.000015, 0.0001, 0.0007, 0.0008  %Magnetostrictive
183      0.00001, 0.2, 0.02, 10000  %' Electroactive Polymer (Macro)'
184      0.001, 0.2, 10, 1000  %' Thermal Bimorph (Macro)'
185      0.01, 1, 10, 1000  %' Pneumatic (Macro)'
186      0.02, 0.03, 800, 8000  %' Hydrolic (Macro)'
187      0.002, 0.003, 1000, 1001  %' State Change (Macro)'
188      0.02, 0.09, 0.1, 20  %' SMA (Macro)'
189      0.001, 0.01, 0.1, 1000  %' Electromagnetic (Macro)'
190      0.000002, 0.001, 0.1, 10000  %' Piezoelectric (Macro)'
191      0.000004, 0.0003, 10000, 1000000  %' Magnetostrictive (Macro)'
192      ];
193
194
195  A_text = {' Discrete energy theory';
196      ' Continuum energy theory';
197      '1 SMA';
198      '2 State Change';
199      '3 Inchworm';
200      '4 Impact Actuator';
```

```
201       '5 Piezoelectric Bimorph';
202       '6 Electromagnetic';
203       '7 Repulsive Force';
204       '8 Curved Electrode';
205       '9 Topology Optimized';
206       '10 Solid Expansion';
207       '11 External Field';
208       '12 Scratch Drive';
209       '13 Thermal Bimorph';
210       '14 Thermal Relay';
211       '15 Distributed Actuator';
212       '16 Electrostatic Relay';
213       '17 Parallel-Plate';
214       '18 Comb Drive';
215       '19 Piezoelectric Expansion';
216       '20 Magnetic Relay';
217       '21 Magnetostrictive';
218       '22 Electroactive Polymer (Macro)';
219       '23 Thermal Bimorph (Macro)';
220       '24 Pneumatic (Macro)';
221       '25 Hydrolic (Macro)';
222       '26 State Change (Macro)';
223       '27 SMA (Macro)';
224       '28 Electromagnetic (Macro)';
225       '29 Piezoelectric (Macro)';
226       '30 Magnetostrictive (Macro)'
227       };
228
229  B = size(A);
230  L=B(1);
231  leg = zeros(1,B(1));
232  leg = transpose(leg);
233  leg = num2str(leg);
234
235  for i=1:L
236  r1 = A(i,1);
```

```
237 r2 = A(i,2);
238 e1 = A(i,3);
239 e2 = A(i,4);
240
241 r_h = [r1/Rad_part, r1/Rad_part, r2/Rad_part, r2/Rad_part, r1/Rad_part];
242 e_h = [e1/(P.*r1.*Rad_part.*pi), e2/(P.*r1.*Rad_part.*pi), e2/(P.*r2.*Rad_part.*pi
243 plot(r_h,e_h,'r','LineWidth',1)
244
245 text(r1/Rad_part,e2/(P.*r1.*Rad_part.*pi),num2str(i))
246 disp(sprintf('%2d. %s\n',i, A_text{i+2}));
247
248
249 % leg(i) = char(A_text{i});
250
251 end
252
253
254 legend(A_text,'Location','EastOutside')
255
256 % leg
257
258 % ENDING ENERGY FUNCTIONALITY
259     end
260
261 end
```

Bibliography

[1] AM Abdalla, DRP Hettiaratchi, and AR Reece. The mechanics of root growth in granular media. *Journal of Agricultural Engineering Research*, 14(3):236–248, 1969.

[2] B Andreotti and L Bonneau. Booming dune instability. *Phys. Rev. Lett.*, 103(238001), 2009.

[3] RA Bagnold. Experiments on a gravity-free dispersion of large solid spheres in a newtonian fluid under shear. *Proc. R. Soc. Lond. A*, 225(1160):49–63, 1954.

[4] RA Bagnold. The flow of cohesionless grains in fluids. *Philosophical Transactions of the Royal Society of London. Series A, Mathematical and Physical Sciences*, 249(964):235–297, 1956.

[5] Werner Baumgartner, Florian Fidler, Agnes Weth, Martin Habbecke, Peter Jakob, Christoph Butenweg, and Wolfgang Böhme. Investigating the locomotion of the sandfish in desert sand using nmr-imaging. *PLoS ONE*, 3(10):e3309, Oct 2008.

[6] RP Behringer. *http://www.phy.duke.edu/∼ bob/*, Bob Behringer's Home Page.

[7] DJ Bell, TJ Lu, NA Fleck, and SM Spearing. Mems actuators and sensors: observations on their performance and selection for purpose. *Journal of Micromechanics and Microengineering*, 15(7):S153–S164, 2005.

[8] AG Bengough. Root responses to soil physical conditions; growth dynamics from field to cell. *Journal of Experimental Botany*, 57(2):437–447, Sep 2005.

[9] IJ Bingham and AG Bengough. Morphological plasticity of wheat and barley roots in response to spatial variation in soil strength. *Plant and Soil*, 250(2):273–282, 2003.

[10] PC Biswal. *Probability and Statistics.* Prentice-Hall, of India Private Limited, New Delhi, 2007.

[11] JF Boudet, Y Amarouchene, B Bonnier, and H Kellay. The granular jump. *J. Fluid Mech.*, 572:413, Feb 2007.

[12] TD Brown and TK Hung. Computational and experimental investigations of two-dimensional nonlinear peristaltic flows. *Journal of Fluid Mechanics*, 83(02):249–272, 1977.

[13] JC Burns and T Parkes. Peristaltic motion. *Journal of Fluid Mechanics*, 29(04):731–743, 1967.

[14] Canon. *www.usa.canon.com.* Lake Success, New York, USA, Canon USA, Inc.

[15] L Cárdenas. New findings in the mechanisms regulating polar growth in root hair cells. *Plant Signaling & Behavior*, 4(1):4, 2009.

[16] ME Cates, JP Wittmer, J-P Bouchaud, and P Claudin. Development of stresses in cohesionless poured sand. *Phil. Trans. R. Soc. Lond. A*, 356(1747):2535–2560, Nov 1998.

[17] CHDK. *chdk.wikia.com/wiki/Software*, Shareware.

[18] P Claudin and J-P Bouchaud. Static avalanches and giant stress fluctuations in silos. *Phys. Rev. Lett.*, 78(2):231–234, 1997.

[19] SN Coppersmith, C Liu, S Majumdar, O Narayan, and TA Witten. Model for force fluctuations in bead packs. *Physical Review E*, 53(5):4673, 1996.

[20] AR Dexter. Mechanics of root growth. *Plant and Soil*, 98(3):303–312, 1987.

[21] M Drew. Soil aeration and plant root metabolism. *Soil science*, 154(4), 1992.

[22] SF Edwards and DV Grinev. Statistical mechanics of stress transmission in disordered granular arrays. *Physical Review Letters*, 82(26):5397–5400, 1999.

[23] RO Erickson and KB Sax. Elemental growth rate of the primary root of zea mays. *Proceedings of the American Philosophical Society*, 100(5):487–498, 1956.

[24] RO Erickson and KB Sax. Rates of cell division and cell elongation in the growth of the primary root of zea mays. *Proceedings of the American Philosophical society*, 100(5):499–514, 1956.

[25] W Fayad, CV Thompson, and HJ Frost. Steady-state grain-size distributions resulting from grain growth in two dimensions. *Scripta materialia*, 40(10):1199–1204, 1999.

[26] Flexinol. *www.dynalloy.com.* Tustin, California, USA, Dynalloy, Inc.

[27] J Geng and R Behringer. Slow drag in two-dimensional granular media. *Phys. Rev. E*, 71(1):011302, 2005.

[28] J Geng, E Longhi, and R Behringer.... Memory in two-dimensional heap experiments. *Phys. Rev. E*, Jan 2001.

[29] LG Gibilaro, K Gallucci, R Di Felice, and P Pagliai. On the apparent viscosity of a fluidized bed. *Chemical Engineering Science*, 62:294–300, 2007.

[30] MA Haque and MTA Saif. Microscale materials testing using mems actuators. *Journal of Microelectromechanical Systems*, 10(1):146–152, 2001.

[31] Harvest. *www.harvestcoop.com.* Boston, Massachusetts, USA, Harvest Cooperative Markets.

[32] T Hayat, Y Wang, K Hutter, S Asghar, and AM Siddiqui. Peristaltic transport of an oldroyd-b fluid in a planar channel. *Math. Probl. Eng.*, 2004(4):347–376, 2004.

[33] AI Hickerson and M Gharib. On the resonance of a pliant tube as a mechanism for valveless pumping. *J. Fluid Mech.*, 555:141, May 2006.

[34] HD Hoeg, AB Slatkin, JW Burdick, and WS Grundfest. Biomechanical modeling of the small intestine as required for the design and operation of a robotic endoscope. *Robotics and Automation, 2000. Proceedings. ICRA'00. IEEE International Conference on*, 2:1599–1606, 2002.

[35] D Howell, RP Behringer, and C Veje. Stress fluctuations in a 2d granular couette experiment: a continuous transition. *Phys. Rev. Lett.*, 82(26):5241–5244, 1999.

[36] TK Hung and TD Brown. Solid-particle motion in two-dimensional peristaltic flows. *Journal of Fluid Mechanics*, 73(01):77–96, 1976.

[37] ML Hunt and NM Vriend. Booming sand dunes. *Annual Review of Earth and Planetary Sciences*, 38:281–301, 2010.

[38] MY Jaffrin and AH Shapiro. Peristaltic pumping. *Annual Review of Fluid Mechanics*, 3(1):13–37, 1971.

[39] P Jop, Y Forterre, and O Pouliquen. A constitutive law for dense granular flows. *Nature*, 441(7094):727–730, Jun 2006.

[40] S Jung. Caenorhabditis elegans swimming in a saturated particulate system. *Physics of Fluids*, 22(031903), 2010.

[41] E Kolb, P Genet, LE Lecoq, C Hartmann, L Quartier, and T Darnige. Root growth in mechanically stressed environment: In situ measurements of radial root forces measured by a photoelastic technique. *6th Plant Biomechanics Conference*, pages 322–327, 2009.

[42] RG Lentle, Y Hemar, and CE Hall. Viscoelastic behaviour aids extrusion from and reabsorption of the liquid phase into the digesta plug: creep rheometry of hindgut digesta in the common brushtail possum trichosurus vulpecula. *J Comp Physiol B*, 176(5):469–475, Jun 2006.

[43] YC Lew and CB Lowenstein. Peristaltic carrying and mixing of chyme in the small intestine (an analysis of a mathematical model of peristalsis of the small intestine). *Journal of Biomechanics*, 4(4):297–315, 1971.

[44] M Li and JG Brasseur. Non-steady peristaltic transport in finite-length tubes. *Journal of Fluid Mechanics*, 248:129–151, 1993.

[45] C Liu, SR Nagel, DA Schecter, SN Coppersmith, S Majumdar, O Narayan, and TA Witten. Force fluctuations in bead packs. *Science*, 269(5223):513–515, July 1995.

[46] EO Macagno and J Christensen. Fluid mechanics of the duodenum. *Annual Review of Fluid Mechanics*, 12(1):139–158, 1980.

[47] TS Majmudar and RP Behringer. Contact force measurements and stress-induced anisotropy in granular materials. *Nature*, 435(23):1079–1082, June 2005.

[48] R Maladen, Y Ding, P Umbanhowar, A Kamor, and D Goldman. Biophysically inspired development of a sand-swimming robot. In *Proceedings of Robotics: Science and Systems*, Zaragoza, Spain, June 2010.

[49] RD Maladen, Y Ding, C Li, and DI Goldman. Undulatory swimming in sand: Subsurface locomotion of the sandfish lizard. *Science*, 325(314):314, 318 2009.

[50] Matlab. *www.mathworks.com/products/matlab/*. Natick, Massachusetts, USA, The MathWorks.

[51] McMaster-Carr. *www.mcmaster.com*. Elmhurst, Illinois, USA, McMaster-Carr Supply Company.

[52] JB McNicholas and PR Rankilor. The mechanical properties of some polyurethane rubbers at room temperature. *Strain*, 5(2):74–79, Apr 1969.

[53] KS Mekheimer, EF El Shehawey, and AM Elaw. Peristaltic motion of a particle-fluid suspension in a planar channel. *International Journal of Theoretical Physics*, 37(11):2895–2920, 1998.

[54] B Miller, C O'Hern, and RP Behringer. Stress fluctuations for continuously sheared granular materials. *Phys. Rev. Lett.*, 77(15):3110–3113, 1996.

[55] RK Misra and AK Gibbons. Growth and morphology of eucalypt seedling-roots, in relation to soil strength arising from compaction. *Plant and soil*, 182(1):1–11, 1996.

[56] D Mueth. Measurements of particle dynamics in slow, dense granular couette flow. *Phys. Rev. E*, 67(1):011304, 2003.

[57] DM Mueth, HM Jaeger, and SR Nagel. Force distribution in a granular medium. *Physical Review E*, 57(3):3164, 1998.

[58] MIT News Office. *http://web.mit.edu/newsoffice//images/articleimages/20100330163823-3.jpg. Cambridge, Massachusetts, USA.*

[59] A Pierret, C Doussan, Y Capowiez, F Bastardie, and L Pagès. Root functional architecture: A framework for modeling the interplay between roots and soil. *Vadose Zone Journal*, 6(2):269, May 2007.

[60] C Pozrikidis. A study of peristaltic flow. *Journal of Fluid Mechanics*, 180:515–527, 1987.

[61] AM Provost and WH Schwarz. A theoretical study of viscous effects in peristaltic pumping. *Journal of Fluid Mechanics*, 279:177–195, 1994.

[62] R Raja. Bounds on life expectancy for the rayleigh and weibull distributions. *Mathematical biosciences*, 96(1):95–115, 1989.

[63] AH Shapiro, MY Jaffrin, and SL Weinberg. Peristaltic pumping with long wavelengths at low reynolds number. *Journal of Fluid Mechanics*, 37(04):799–825, 1969.

[64] LE Silbert, D Ertas, GS Grest, TC Halsey, D Levine, and SJ Plimpton. Granular flow down an inclined plane: Bagnold scaling and rheology. *Phys. Rev. E*, 64(051302), 2001.

[65] WK Silk and JMH Beusmans. Mechanical properties within the growth zone of corn roots investigated by bending experiments. i. preliminary observations. *American Journal of Botany*, 75(7):990–995, 1988.

[66] D Srinivasacharya, M Mishra, and AR Rao. Peristaltic pumping of a micropolar fluid in a tube. *Acta Mechanica*, 161(3):165–178, 2003.

[67] LM Srivastava and VP Srivastava. Peristaltic transport of a particle-fluid suspension. *Journal of biomechanical engineering*, 111(2):157, 1989.

[68] VP Srivastava and LM Srivastava. Effects of poiseuille flow on peristaltic transport of a particulate suspension. *Zeitschrift für Angewandte Mathematik und Physik (ZAMP)*, 46(5):655–679, 1995.

[69] S Takabatake, K Ayukawa, and A Mori. Peristaltic pumping in circular cylindrical tubes: a numerical study of fluid transport and its efficiency. *Journal of Fluid Mechanics*, 193:267–283, 1988.

[70] TA.XT.Plus. *www.texturetechnologies.com.* Scarsdale, New York, USA, Texture Technologies Corporation.

[71] Water. *www.polandspring.com.* Wilkes Barre, Pennsylvania, USA, Poland Spring Water.

[72] W Weems. Intestingal wall motion, propulsion, and fluid movement - trends toward a unified theory. *Am J Physiol*, 243(3):G117–G188, 1982.

[73] Q Xiao and M Damodaran. A numerical investigation of peristaltic waves in circular tubes. *Int. J. of Computational Fluid Dynamics*, 16(3):201–216, 2002.

[74] J Zhang. *http://www.aps.org/about/physics-images/archive/chains.cfm*, American Physical Society.

[75] J Zhang, T Majmudar, A Tordesillas, and R Behringer. Statistical properties of a 2d granular material subjected to cyclic shear. *Granular Matter*, 12:159–172, 2010.

[76] JWL Zhou, H-Y Chan, TKH To, KWC Lai, and WJ Li. Polymer mems actuators for underwater micromanipulation. *IEEE/ASME Transactions on Mechatronics*, 9(2):334–342, 2004.

[77] C Zou, C Penfold, R Sands, RK Misra, and I Hudson. Effects of soil air-filled porosity, soil matric potential and soil strength on primary root growth of radiata pine seedlings. *Plant and Soil*, 236(1):105–115, 2001.

[78] C Zou, R Sands, and O Sun. Physiological responses of radiata pine roots to soil strength and soil water deficit. *Tree physiology*, 20(17):1205, 2000.

[79] I Zuriguel, A Garcimartin, LA Pugnaloni, and JM Pastor. Jamming during the discharge of granular matter from a silo. *Phys. Rev. E*, 71(051303), 2005.